Ocean Engineering 266 (2022) 113127

Contents lists available at ScienceDirect

Ocean Engineering

journal homepage: www.elsevier.com/locate/oceaneng

Ship design for real sea states under uncertainty

Ehsan Esmailian [a,*], Sverre Steen [a], Kourosh Koushan [a,b]

[a] Department of Marine Technology, Norwegian University of Science and Technology (NTNU), Trondheim, Norway
[b] Department of Ship and Ocean Structures, SINTEF Ocean AS, 7465 Trondheim, Norway

ARTICLE INFO

Keywords:
Ship design
Real sea state
Robust optimization
Aleatory uncertainty
Epistemic uncertainty
Slow steaming
Green shipping

ABSTRACT

A ship is designed under inescapable uncertainty. Neglecting important uncertainties might lead to suboptimal designs. Furthermore, to achieve the best possible performance, the ship design should be optimized for the actual operational conditions, not just for calm water at design speed. This paper aims to propose a two-stage method for the optimal design of ships under uncertainty, operating at various speeds in real sea states, addressing both aleatory uncertainties due to the weather and epistemic uncertainties due to the model and methodology. A general cargo ship is used as a test case. A comparison with different cases representing traditional approaches for optimizing the ship design is provided. The effect of the slow steaming speeds on the design is studied. Results indicate the effectiveness of the adopted approach to deal with the epistemic and aleatory uncertainties in all cases studied. Verification with in-service data confirms the effectiveness of the suggested approach. Furthermore, epistemic and aleatory uncertainties resulted in up to 26.91% reductions in the average attainable speed of different cases compared to the optimal case.

1. Introduction

While accounting for more than 90% of global trade, shipping is responsible for more than 10% of global NO_x emissions, 1–3% of SO_x emissions, and approximately 3% of CO_2 emissions. As transportation demand increases, these emissions are projected to increase by 150–200% by 2050 (Smith et al., 2015). The development of more energy-efficient ships is driven by the increasing pressure on the shipping industry to reduce its environmental impact.

In 2018, the International Maritime Organization (IMO) adopted a strategy to reduce maritime greenhouse gas (GHG) emissions by at least 50% by 2050, reduce carbon intensity (CI) by 40% by 2030 and decarbonize by 70% by 2050 (Resolution, 2018). For compliance with these regulations, various technologies have been explored, including LNG fuel technology, solar energy technology, battery power technology, wind energy technology, hydrogen fuel technology, ammonia fuel technology, etc (Ren and Lützen, 2015; Xuan et al., 2022). In the midst of the continuous advance of clean energy technologies and the continuous increase of potential applications, applying new technologies to ships is becoming increasingly complicated as we move into the future. However, regardless of the ship type and which technology will be implemented, hydrodynamically improving the ship performance, as a viable way to reduce energy consumption and the associated emissions and costs, is always crucial for either current and future ships.

Uncertainty is an unavoidable aspect of ship design. Ignoring the inherent uncertainty of parameters in real navigation might have a detrimental effect on the design, with certain hidden dangers in practice (Wei et al., 2019). In recent years, uncertainty-based design optimization (UDO) has been continuously developed and broadly used in ship design. A groundbreaking study into the impact of uncertainties on the ship design was conducted by Diez et al. (2010). In that study, Robust Design (RD) and Robust Optimization Design (ROD) are suggested as effective ways to optimize the main dimensions of a container ship. Thereafter, multiple studies have been conducted to develop RD and ROD strategies for ship hull Simulation-Based Design (SBD) systems; from principal dimensions to hull lines (Wei et al., 2013; Diez et al., 2014; Hou et al., 2021a; Coppedè et al., 2019), single uncertain parameter to multiple (Leotardi et al., 2015), speed disturbance to wave response (Chen et al., 2015), introducing uncertainty into constraint conditions (Hannapel and Vlahopoulos, 2010), reducing the design space (Hou et al., 2021b; D'Agostino et al., 2020; Serani and Diez, 2018; Serani et al., 2019).

The uncertainty in the ship design can be divided into two categories – aleatory and epistemic. The aleatory uncertainty is irreducible and is due to the natural randomness of random variables, such as weather. The epistemic uncertainty is due to the lack of knowledge and can be reduced by accumulating more information and improving the applied models (Hang Hou et al., 2019). In another category, ship design uncertainty is divided into the following elements (Nikolopoulos and Boulougouris, 2018):

* Corresponding author.
E-mail addresses: ehsan.esmailian@ntnu.no (E. Esmailian), sverre.steen@ntnu.no (S. Steen), kourosh.koushan@sintef.no (K. Koushan).

https://doi.org/10.1016/j.oceaneng.2022.113127
Received 6 September 2022; Received in revised form 25 October 2022; Accepted 6 November 2022
Available online 26 November 2022

Nomenclature

$\frac{A_e}{A_o}$	Expanded area ratio
A_{XV}	Transverse projected area above the waterline
B	Ship beam
c	Chord length
C_{AA}	Wind resistance coefficient
$C^{Q}_{s,t,u,v}$	Regression coefficient for torque
$C^{T}_{s,t,u,v}$	Regression coefficient for thrust
C_B	Block coefficient
C_{DM}	Model drag coefficient for the blade section
C_M	Midship section coefficient
C_{SD}	Speed-dependent constraint
$\bar{C}_{SD}$	Average of C_{SD} over the long term
C_{WP}	Waterplane area coefficient
d	Ship draft
D_p	Propeller diameter
$\bar{F}_{Obj}$	Objective function over the long term
GM	Metacentric height
GZ	Righting lever
H_s	Significant wave height
J	Advance coefficient
KG	Vertical center of gravity above the keel
k_p	Propeller roughness
K_Q	Torque coefficient
K_T	Thrust coefficient
L_{pp}	Length between perpendiculars
m_n	Total number of probability variables
n	Rotational speed of the propeller
$\bar{n}$	Average rotational speed of the propeller over the long term
$n_{P^{tot}_{Enc}}$	Number of probability values of β
n_{P_P}	Number of probability values of P_s
n_{rpm}	Propeller rpm
$n_{P_{SD}}$	Number of probability values of the pair of H_s and T_p
n_{Zone}	Number of zones contributing the voyage
P_b	Brake power
$P^{Calm}_{Cav_{lim}}$	Probability of occurring cavitation in calm water
$P^{Sea}_{Cav_{lim}}$	Probability of occurring cavitation in seaway
P_E	Effective power
P^{tot}_{Enc}	Encounter wave probability for the entire voyage
$P^{Calm}_{Eng_{lim}}$	Probability of exceeding engine limits in calm water
$P^{Sea}_{Eng_{lim}}$	Probability of exceeding engine limits in seaway
P_s	Shaft power
$P_{s_{Opr}}$	Operation shaft power
P_{P_s}	Probability of the shaft power
$P_{s_{Cal}}$	Calculated shaft power
P_{SD}	Probabilities of the pair of H_s and T_p
P_V	Vapor pressure
P^{i}_{Zone}	Contribution of zone i over the entire route
P_0	Atmospheric pressure
Pr	Probability value in percent
$Pr^{RSS}_{Cav_{lim}}$	Probability of occurring cavitation in RSS
$Pr^{RSS}_{Eng_{lim}}$	Probability of exceeding engine limit in RSS
$\frac{P}{D_p}$	Pitch ratio
R_{AW}	Added resistance in irregular waves
R_{aw}	Added resistance in waves
R_{Calm}	Calm water resistance
Re_{c0}	Model Reynolds number
R_{Wind}	Added resistance due to the wind
R_T	Total resistance
$\bar{R}_T$	Average total resistance over the long term
s	Power exponent
S_{wet}	Wetted surface area
S	Wave spectrum
SD^{i}_{wave}	Wave scatter of zone i
SD^{Voy}_{wave}	Wave scatter for voyage
t	Power exponent
T_p	Peak wave period
T_C	Calculated thrust
t_p	Thrust deduction factor
T_R	Required thrust
u	Power exponent
v	Power exponent
V_A	Mean axial advance velocity
V_d	Design speed
V_S	Ship forward speed
$\bar{V}^{Opt}_S$	Average speed over the long term obtained from optimization process
V_{WRref}	Relative wind velocity at the reference height
V_{WTref}	Corrected true wind velocity
w	Wake factor
Z	Number of blades
z_G	Vertical center of gravity above waterline
β	Encounter wave angle
Δ	Ship displacement
η_D	Propulsive efficiency
η_H	Hull efficiency
η_o	Open water efficiency
η_R	Relative rotative efficiency
η_S	Shaft efficiency
η_T	Total propulsive efficiency
∇	Ship displacement volume
ω	Wave frequency
ψ	Ship heading
ψ_{WRref}	Relative wind direction at the reference height
ψ_{WT}	True wind direction
ρ_{air}	Density of air
ζ_a	Wave amplitude

(i) Weather and Environmental Uncertainties
(ii) Methodology Uncertainty and Error Modeling
(iii) Shipping Market Uncertainties

The study of the shipping market uncertainties is not the purpose of the current work, and the methodologies to deal with the first two elements will be discussed.

Depending on the environment, a ship might change her route to improve energy efficiency, voyage duration, safety, or combinations of these aspects. If a ship is not properly designed with regard to the operating envelope, she might experience significant voluntary/involuntary speed losses, as well as significant power fluctuations, which can negatively affect both her mechanical and electrical systems (Perez et al., 2006; Sørensen and Smogeli, 2009; Smogeli and Sørensen, 2009). These factors will increase mechanical stress and consequently wear and tear (Smogeli, 2006; Radan, 2008; Wei et al., 2019). Fluctuations in power can also result in a reduction in electrical efficiency, excessive power consumption, or even degradation of the power quality of the shipboard power network (McCarthy, 1961; Koushan et al., 2007; Radan, 2008; Sørensen and Smogeli, 2009; Smogeli and Sørensen, 2009; Wei et al., 2019). For the purpose of maximizing the energy efficiency of a ship in a seaway, there is a necessity to suggest designs robust in the presence of varying ship environments and weather conditions, referring to "aleatory" uncertainties in this study.

Probabilistic-based approaches are regarded as a viable way to handle aleatory uncertainties (Priftis et al., 2020). In the literature, several studies can be found employed probabilistic-based approaches to find the optimal design of ships within an operating envelope. The trade-off between manufacturing complexity and resistance was investigated by Temple and Collette (2012) based on a probabilistic ship speed profile. Using a probabilistic ship speed profile, researchers recommend optimizing a Series-60 ship hull with a B-series propeller to reduce a ship's lifetime fuel consumption (LFC) (Esmailian et al., 2017). The research published by Esmailian et al. (2019) suggests that an integrated photovoltaic (PV)-hull-propeller system could be used to optimize a boat design based on a probabilistic ship speed profile. According to Kramer et al. (2010), speed and sea state were integrated into a probabilistic technique for enhancing waterjet efficiency by modifying the diameter. In that study, life-cycle efficiency was found to increase by 3%–10% using probabilistic techniques. A similar investigation by Motley and Young (2011) was conducted to examine the benefits of composite propellers versus nickel–aluminum–bronze propellers. Motley et al. (2012) proposed a probability-based strategy to reduce the LFC by enhancing the propulsion efficiency. Based on the optimization of the hull-propeller system of a KCS container ship, the LFC was reduced using the probabilistic speed technique (Nelson et al., 2013). Referring to Ralph (2016), a probabilistic approach was applied to deal with uncertainties due to ice and iceberg impact loads. In the preliminary ship design, Bayesian networks were used to obtain the probability distributions for the relations among the ship's main characteristics, such as the ship length, breadth, depth, draft, speed, displacement, block coefficient, and loading capacity (Clausen et al., 2001). Referencing (Zaman et al., 2011), various approaches to handle uncertainties are reviewed, and then a probabilistic framework is proposed to jointly handle aleatory and epistemic uncertainties. In Li et al. (2021), a probabilistic framework is proposed to deal with the uncertainty caused by the variation in the load-shortening curve (LSC) of a hull girder. According to Nikolopoulos and Boulougouris (2020), probabilistic approaches are proposed to deal with environmental and market-related uncertainties associated with ship design. A probabilistic approach based on the ship power profile was suggested by Esmailian and Steen (2022) for designing ships in real sea states. In comparison to the design of ships in calm water with constant design speed, that approach was found to be effective in the design of a container ship at sea. The potential of an approach similar to that is examined here to reduce aleatory uncertainties caused by the weather.

There are several assumptions and simplifications made in order to provide a model to assess different aspects of ship design, particularly at the early design stages, leading to a higher level of uncertainty. However, there is still a lack of quantification of expected prediction accuracy and a better understanding of the ways to handle this type of uncertainty (Tillig et al., 2018), which are referred to as "epistemic uncertainty" in this research. In this paper, we aim to give an estimate of the uncertainty of the power prediction and suggest a method to minimize this uncertainty, as the accuracy of the power prediction is believed to be of critical importance to the ship design optimization method that is applied in the current work.

When one examines a ship operation over an extended period of time, several weeks or more, one notices that both speed and power vary significantly and that they are (as expected) closely correlated. Thus, the designer may express the probability of the ship speed using either the speed profile or the power profile. However, one might observe that speed and sea state are inextricably correlated, higher sea states often result in slower speeds. This is less evident in the case of power, as power is often kept relatively constant regardless of the weather, as long as conditions do not require voluntary speed losses. Different stochastic variables should ideally be uncorrelated in a probabilistic method (or else the correlation must be taken into account, which is challenging). As a result, this research suggests a probabilistic-based strategy based on the ship power profile rather than the speed profile for dealing with aleatory uncertainty arisen by the environment. Instead, the resulting speed is estimated indirectly, based on the weather and input power.

In this study, we introduce a two-stage approach for designing ships under uncertainty in real sea states. In the *first stage*, by comparing the results of the power prediction model and ship-in service data for a reference vessel (or parent hull), a normalized root mean square error (NRMSE) is defined. Then, a tuning optimization problem is developed to minimize the NRMSE to find the optimal combination of methods used to calculate different components of the ship power (calm water resistance, added resistance in wind and waves, wetted surface, wake, etc.), resulting in a more accurate power prediction model and thus reducing epistemic uncertainties.

The *second stage* applies the power prediction model obtained from the *first stage*. Then, a probability-based optimization method is suggested, with the ship power profile and environmental characteristics (wave and wind angles, significant wave height, mean wave period, and wind speed) defined as probability variables and the achievable speed over the long term as the optimization objective. This is an attempt to design ships with a higher average achievable speed under unpredictable environments, resulting in more energy-efficient ships at sea. A short-term analysis is also included to evaluate the performance of the suggested approach. As a test case, a general cargo ship is used to evaluate the performance of the proposed approach. A comparison analysis with the traditional methods is presented to highlight the effectiveness of the suggested approach.

In the following, the proposed approach is described in Section 2. The suggested approach is tested on a general cargo ship in Section 3. The results are summarized in Section 4. The conclusion is presented in Section 5.

2. Ship design under uncertainty

2.1. Epistemic uncertainties

As indicated previously, substantial epistemic uncertainty may be incorporated into the ship design problem as a result of the assumptions and simplifications made, but there is still a lack of quantification in terms of the prediction accuracy and the understanding of how to address it (Tillig et al., 2018). In the following, we will discuss the methods used for calculating different components of the ship power prediction model. Then, the tuning approach developed to find an optimal combination of methods for predicting the ship power is explained.

2.1.1. Method selection

This part will go through the methods for computing various components of the power prediction model, such as calm water resistance, added resistance in wind and waves, wetted surface area, and so on. Several criteria may be considered while selecting approaches, including adaptability to a wide variety of ship types, high accuracy, computational simplicity, and minimal input. The methods applied for calculating different parameters are discussed in the following sections. The primary goal of this study is to demonstrate the potential of the proposed technique in minimizing epistemic uncertainty. However, based on the designer's decision, the strategy proposed in this paper can be expanded to cover more parameters and methodologies to achieve even better results.

2.1.1.1. Resistance

Ship design studies have largely focused on the design of ships for calm water conditions, despite the fact that a ship rarely operates in calm water and her performance might vary significantly in real sea states. It is then necessary to estimate the added resistance based on the different environments experienced by the ship. In this study, the added resistances due to waves and winds are considered. As a result, the ship's total resistance is defined as

$$R_T = R_{Calm} + R_{AW} + R_{Wind} \tag{1}$$

where R_{Calm}, R_{AW}, and R_{Wind} denote the calm water resistance, the added resistance in waves, and the added resistance due to the wind, respectively. Maneuvering and the use of the rudder will also contribute to increasing in resistance. However, these are generally of less importance and therefore ignored in the current work.

2.1.1.1.1. Calm water resistance

The updated Guldhammer-Harvald (GH) (2017), Holtrop–Mennen (HM) (1984), and Hollenbach (HB) (1998) are the methods considered for calculating the calm water resistance. All techniques give regression-based formulas based on a comprehensive study of model testing and are widely used today. Holtrop–Mennen's method has the largest applicable range, hence it is appropriate to include it. Hollenbach's research suggests that Holtrop–Mennen's and Hollenbach's methods are more accurate than the original Guldhammer–Harvald's approach. Both Hollenbach's and Holtrop–Mennen's methods are therefore suitable. However, because Kristensen et al. (2017) have upgraded Guldhammer–Harvald's approach to match modern ships, it is also appropriate to include it. Holtrop–Mennen's approach has fewer restrictions than Guldhammer–Harvald's and Hollenbach's methods. Nevertheless, all three are anticipated to apply to conventional cargo vessels. To calculate the resistance through Hollenbach's methodology, the mean line is used. The tuning method also includes the mean value of calm water resistance derived from the combination of GH & HM, GH & HB, and HM & HB.

2.1.1.1.2. Added resistance in waves

Through numerical integration of a series of regular waves with frequency ω and wave amplitude ζ_a for a given peak wave period T_p, wave heading, and significant wave height H_s, the mean added resistance in the irregular waves is obtained as follows

$$R_{AW} = 2\int_0^{2\pi}\int_0^{\infty} S(\omega)\,\frac{R_{aw}(\omega,\beta,V_S)}{\zeta_a^2}\,d\omega\,d\beta \tag{2}$$

The best appropriate spectrum is chosen based on the vessel route and will vary throughout the fleet. JONSWAP is often used in coastal waters. The modified Pierson–Moskowitz (Bretschneider) wave spectrum is used in the current study since it is considered that most ships operate in the deep sea with a fully developed sea condition. It is defined as follows

$$S(\omega) = \frac{A_{fw}}{\omega^5} exp(\frac{-B_{fw}}{\omega^4}) \tag{3}$$

where

$$A_{fw} = 173\frac{H_s^2}{T_p^4} \tag{4}$$

and

$$B_{fw} = \frac{692}{T_p^4} \tag{5}$$

R_{aw} in Eq. (2) is the frequency-dependent added resistance due to waves. Several different methods to calculate R_{aw} exist. This section discusses which strategies should be included in the power prediction model. ISO 15016 recommends STA-1 and STA-2 for all types of ships (ISO, 2015). The STA-1 is restricted to moderate sea conditions. As a result, STA-2 has been developed to enhance its applicability in higher sea states. Both STA-1 and STA-2 are only valid for head sea (+−45 deg off bow), implicitly assuming zero added resistance for other headings. Recently, different methods such as CTH (Lang and Mao, 2021), SNNM (Liu and Papanikolaou, 2020), and Combined (Kim et al., 2022) approaches were proposed that performed significantly better in nearly all comparison cases than STA2, and they have the advantage of estimating results for arbitrary wave headings as well. Since these methods require only a limited amount of hull form information, they can be applied when detailed hull forms are not available. Therefore, CTH, SNNM, and Combined methods are chosen here. There are of course a large number of numerical methods to compute added resistance, but due to the general need for detailed hull form information, as well as computational time and also a lack of robustness in numerical methods, such methods are not included in the present work.

2.1.1.1.3. Added resistance due to wind

Wind resistance is dependent on the wind speed and the area above the waterline. In ships with large volumes above the waterline, the wind resistance contributes significantly to the total resistance. The added resistance due to wind can be written as follows (ISO, 2015)

$$R_{wind} = 0.5\rho_{air}\cdot C_{AA}(\psi_{WRref})\cdot A_{xv}\cdot V_{WRref}^2 - 0.5\rho_{air}\cdot C_{AA}(0)\cdot A_{xv}\cdot V_S^2 \tag{6}$$

$$V_{WRref} = \sqrt{V_{WTref}^2 + V_S^2 + 2\cdot V_{WTref}\cdot V_S\cdot cos(\psi_{WT}-\psi)} \tag{7}$$

Both wave and wind are assumed to be pointing in the same direction. Hence, $\beta = \psi_{WT} - \psi$. Also, the wind speed V_{WTref} is provided by Stewart (2008) as follows

$$V_{WTref} = \sqrt{\frac{gH_s}{0.22}} \tag{8}$$

To estimate the wind resistance coefficients C_{AA}, model tests conducted in a wind tunnel or CFD calculations might be used, or coefficients might be obtained from tabulated data, which typically are based on previous tests with similar ship shapes. In absence of wind tunnel tests or CFD calculations, Blendermann (1995) and ISO (2015) are extensively employed and expected to yield reliable estimates of wind resistance coefficients. In the study, these two methods are thus included in the tuning approach.

2.1.1.2. Propulsion system

The total propulsive efficiency η_T is found by

$$\eta_T = \eta_H\eta_o\eta_R\eta_S \tag{9}$$

In order to evaluate the propeller performance in the preliminary design stage, the Wageningen B-screw series is commonly used (Oosterveld and van Oossanen, 1975). The series includes open fixed pitch propellers with blade area ratios of 0.30 to 1.05, pitch ratios of 0.5 to 1.4, and from 2 to 7 blades. The open water characteristics of the Wageningen B-screw series are described with polynomials obtained

based on a regression analysis performed on the test results of 120 propeller models of the B-screw series. The following regression formulas for thrust and torque coefficients of B-series propellers are applied

$$K_T = \Sigma C^T_{s,t,u,v}(J)^s(\frac{P}{D_p})^t(\frac{A_e}{A_o})^u(Z)^v \tag{10}$$

$$K_Q = \Sigma C^Q_{s,t,u,v}(J)^s(\frac{P}{D_p})^t(\frac{A_e}{A_o})^u(Z)^v \tag{11}$$

where the regression coefficients $C^Q_{s,t,u,v}$ and $C^T_{s,t,u,v}$ and exponents s, t, u, and v are found based on the data presented in Oosterveld and van Oossanen (1975). The advance coefficient, J, is expressed as

$$J = \frac{V_A}{nD_p} \tag{12}$$

where V_A is given by

$$V_A = V_S(1-w). \tag{13}$$

The open water efficiency is written as

$$\eta_o = \frac{K_T J}{K_Q 2\pi}. \tag{14}$$

Following are the formulas that determine the required thrust T_R and the calculated thrust T_C

$$T_C = K_T \rho n^2 D_p^4, \tag{15}$$

$$T_R = \frac{R_T}{1-t_p} \tag{16}$$

Matching the calculated thrust with the required thrust is essential for the design of a propeller. For this purpose, the thrust coefficient is rewritten as

$$K_T = \frac{T_R}{\rho n^2 D_p^4} = AJ^2 \tag{17}$$

where $A = \frac{K_T}{J^2}$ is defined to remove the unknown revolution rate as follows

$$A = \frac{T_R}{\rho V_A^2 D_p^2}. \tag{18}$$

The wake factor, thrust deduction factor, and relative rotative efficiency are obtained based on the same method used to calculate the calm water resistance. The shaft efficiency $\eta_S = 0.98$ is assumed (Kristensen and Lützen, 2012). Having the ship resistance, the wake factor, and the thrust deduction factor, one can calculate the parameter A at different speeds. Then, the intersection point between $K_T(J)$ in (17) and $K_T(J)$ from the propeller open water diagram gives the advance coefficient and propeller open water efficiency. Note that even if the wake and thrust deduction factors might be influenced by operation in waves, this effect is not accounted for here.

The K_T and K_Q values determined during the open water test should not be applied directly to the full-scale vessel. Model propellers have a lower Reynolds number than full-scale propellers, leading to different viscous effects in the model and full scale. As a result, the thrust and torque coefficient polynomials should be corrected to account for the full scale Reynolds number. The correction can be performed by the ITTC approach (ITTC, 2014), in which the full scale thrust and torque are calculated as follows

$$K_{Ts} = K_T - \Delta K_T \tag{19}$$

$$K_{Qs} = K_Q - \Delta K_Q \tag{20}$$

where

$$\Delta K_T = -\Delta C_D \cdot 0.30 \cdot \frac{P}{D_p} \cdot \frac{c \cdot Z}{D} \tag{21}$$

$$\Delta K_Q = \Delta C_D \cdot 0.25 \cdot \frac{c \cdot Z}{D_p} \tag{22}$$

The difference in drag coefficient ΔC_D is

$$\Delta C_D = C_{Dm} - C_{Ds} \tag{23}$$

where

$$C_{Dm} = 2 \cdot \left(1 + 2\frac{t}{c}\right) \cdot \left[\frac{0.044}{(Re_{c0})^{\frac{1}{6}}} - \frac{5}{(Re_{c0})^{\frac{2}{3}}}\right] \tag{24}$$

and

$$C_{Ds} = 2 \cdot \left(1 + 2\frac{t}{c}\right) \cdot \left(1.89 + 1.62 \cdot \log_{10}\frac{c}{k_p}\right)^{-2.5} \tag{25}$$

where Re_{c0} is computed as follows

$$Re_{c0} = \frac{c_{0.75R}}{\nu} \cdot \sqrt{{V_0}^2 + (0.75\pi nD)^2} \tag{26}$$

2.1.1.3. Hydrostatic parameters

The hydrostatic parameters of a ship can be determined through numerical calculations or regression-based formulas. As an assumption, this study investigates the effects of numerical calculations and regression formulas for calculating the wetted surface area, the midship section and waterplane area coefficients. A reason for including those parameters in the tuning approach is that they are in the category of input parameters that are either calculated numerically or via the regression formula in a power prediction model. As a result, the study of the effects of uncertainties coming from different approaches (numerical calculations or regression-based formulas) used to compute those parameters is interesting. In order to calculate them numerically, the ship offset table is used. In addition, they are computed through the following well-known regression-based formulas.

Mumford's formula (Kristensen and Lützen, 2012):

$$S_{wet} = 1.025 \cdot (\frac{\nabla}{d} + 1.7 \cdot L_{PP} \cdot d) \tag{27}$$

Papanikolaou (2014):

$$C_{WP} = \frac{1 + 2C_B}{3} \tag{28}$$

Schneekluth and Bertram (1998):

$$C_M = 0.93 + 0.08C_B \tag{29}$$

Other hydrostatic parameters are computed numerically through the ship offset.

2.1.2. Shaft power

With the resistance of the ship and the efficiency of the propulsion system in hand, the shaft power can be calculated as follows

$$P_{sCal} = \frac{R_T V_S}{\eta_T} \tag{30}$$

Once R_T and η_T are known, P_{sCal} can be determined by (30) for a given ship speed.

2.1.3. Tuning approach

In this section, a tuning optimization approach is proposed to reduce the epistemic uncertainty caused by the assumptions and simplifications used in developing a power prediction model. A simple schematic of the proposed approach is shown in Fig. 1. The proposed method entails determining the optimal combination of the explored methods for analyzing various components of a ship design in order to predict the ship power. This is accomplished by defining the normalized mean root square error (NRMSE) as the difference between the estimated power from the model and the actual power determined from the ship in-service data. $NRMSE$ is defined by

$$NRMSE = \frac{RMSE}{MCR} \tag{31}$$

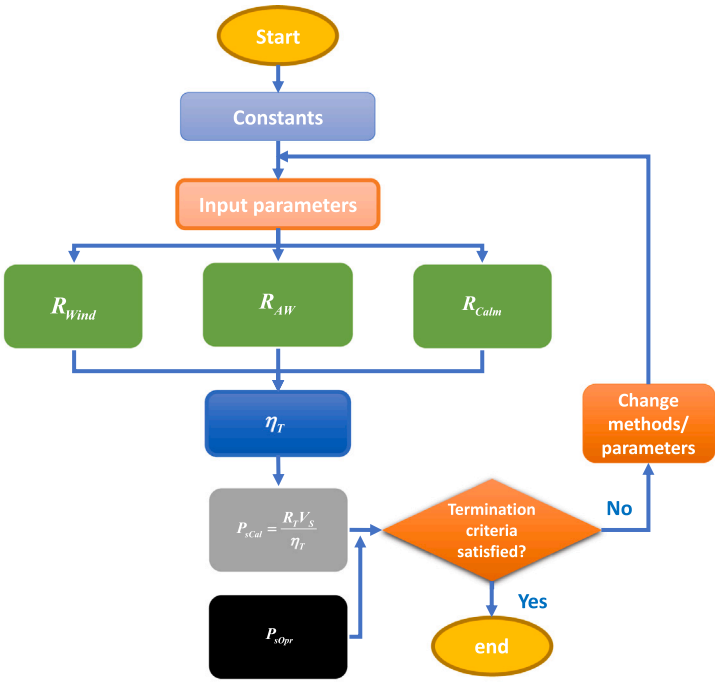

Fig. 1. A simple schematic of the power prediction optimization model.

with

$$RMSE = \sqrt{\frac{\sum_{i=1}^{n}(P_{sCal} - P_{sOpr})^2}{n}} \tag{32}$$

where P_{sCal} and P_{sOpr} denote the calculated shaft power and the shaft power estimated from ship in-service data, respectively. The method might also be applied to other performance data than in-service data, as long as the data is sufficiently accurate and cover a sufficiently large range of variation of the parameters of interest. Additionally, MCR and n represent the engine maximum continuous rating and the number of samples, respectively. The resulting NRMSE is then minimized using a tuning optimization problem to identify the optimal combination of approaches to achieve a more accurate power prediction model and thereby lowering epistemic uncertainty. Here, the surrogate optimization strategy in Matlab is utilized, which is recommended for time-consuming objective functions in order to shorten the computational time (MathWorks, 2022). When the tuning algorithm reaches the function evaluation limit or when the computed objective function value of a feasible point is less than the objective function value tolerance, the tuning algorithm terminates. In Esmailian et al. (2022), the applied power prediction method is discussed in detail.

2.2. Aleatory uncertainties

As discussed earlier, probabilistic-based approaches are regarded as a viable way to handle aleatory uncertainties. Here, a probability-based optimization method is proposed for coping with the aleatory uncertainty arising from the environment, with the ship power profile and environmental characteristics (wave and wind angles, significant wave height, mean wave period, and wind speed) defined as probability variables and the achievable speed over the long term ($\bar{V}_S^{Opt}$) as the optimization objective. Then, the aim is to design ships with higher average achievable speeds under unpredictable environments, resulting in more energy-efficient ships at sea and less aleatory uncertainty. The attainable ship speed over the long term $\bar{V}_S^{Opt}$ is defined as

$$\bar{V}_S^{Opt} = \iiiint P_{Enc}^{tot}(\beta)\, P_{SD}(H_S, T_p)\, P_P(P_s)\, V_s\, d\beta\, dT_p\, dH_s\, dP_s. \tag{33}$$

Fig. 2 illustrates the procedure to calculate the integral above. The inner loop in that figure stops when the absolute difference between the operation engine power $P_{s_{Opr}}$ and the calculated brake power $P_{s_{Cal}}$ is less than 0.1% of $P_{s_{Opr}}$ and then the ship speed V_S and speed-dependent constraint C_{SD} corresponding to a given power and environment condition (denoted by the index of j) are calculated. Here, $P_{s_{Cal}}$ is determined using the model obtained from Section 2.1. Once the total number of probability values $m_n = n_{P_{Enc}^{tot}}\, n_{P_{SD}}\, n_{P_P}$ is reached, the middle loop terminates and the average speed over the long term $\bar{V}_S^{Opt}$ as well as the average speed-dependent constraints over the long term $\bar{C}_{SD}$ are obtained. Here, $n_{P_{Enc}^{tot}}$, $n_{P_{SD}}$, and n_{P_P} are the numbers of probability values for the encounter wave angle β, the pair of H_s and T_p, and the ship shaft power P_s, respectively. The procedures to calculate the probabilities of the shaft power P_P, encounter wave and wind angle P_{Enc}^{tot}, and significant wave height and mean wave period P_{SD} along with the speed-dependent constraints will be discussed in the upcoming sections. Finally, the outer loop aims to find the optimal ship design. In order to accomplish this, the decision variables are changed and optimization constraints are checked by an optimization algorithm. The optimization algorithm continues until the termination criteria are met and the optimal design with the maximum attainable ship speed over the long term, $\bar{V}_S^{Opt}$, is found. The proposed approach will be exemplified in Section 3.3.

2.2.1. Probability of power

The power profile of a ship describes the probability of the ship operating at various levels of power. In-service reports of similar ships with the same mission or knowledge of the ship's operation can provide insight into the ship power profile. It is also possible to develop a power profile based on knowledge of the planned operation. As an example, Fig. 3 shows the power profile obtained from the in-service data of a general cargo ship over the period 2014–2019.

2.2.2. Probabilities of significant wave height and mean wave period

When designing a ship, it is crucial to have a reliable prediction of the sea conditions expected to be experienced by the ship over her lifetime. For this purpose, a scatter diagram is useful to consider the probability of weather conditions varying across the operating

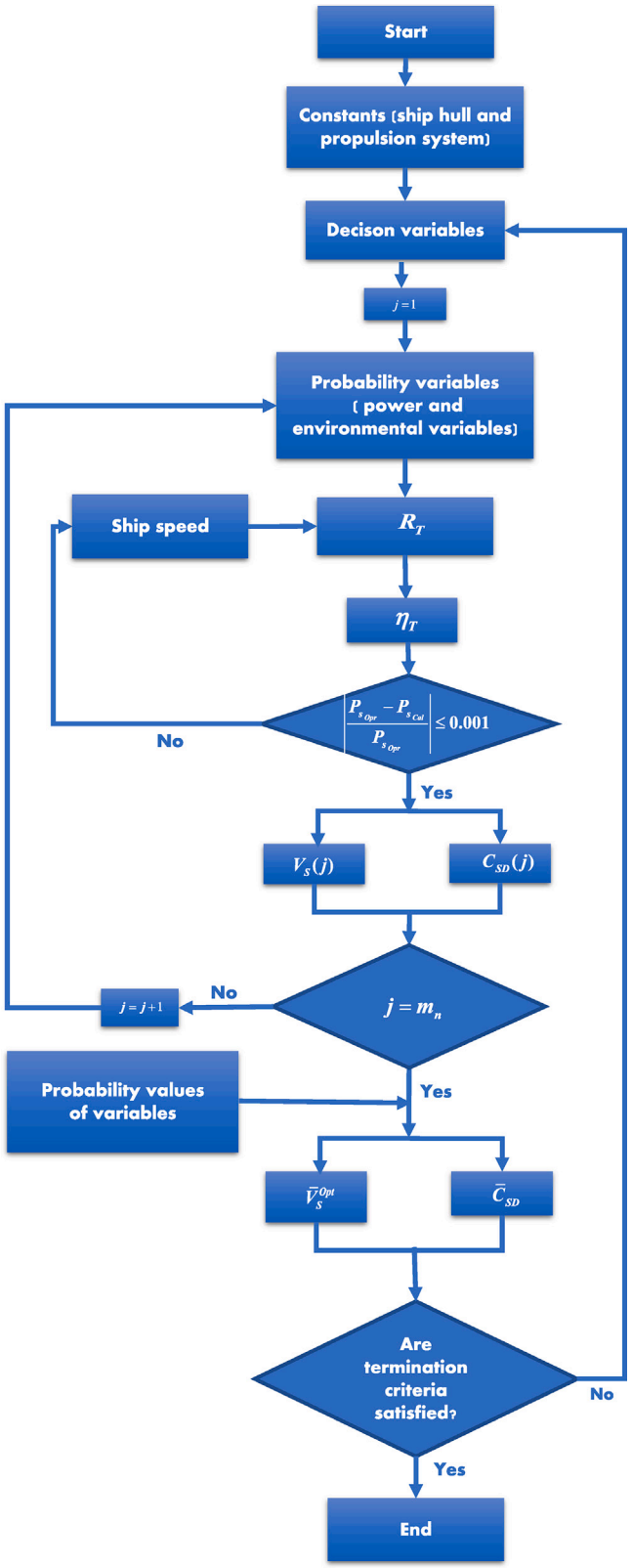

Fig. 2. Flowchart of the suggested approach for the ship design optimization.

area. Through scatter diagrams, the wave climate is summed up and expressed as the probabilities of significant wave heights and the mean

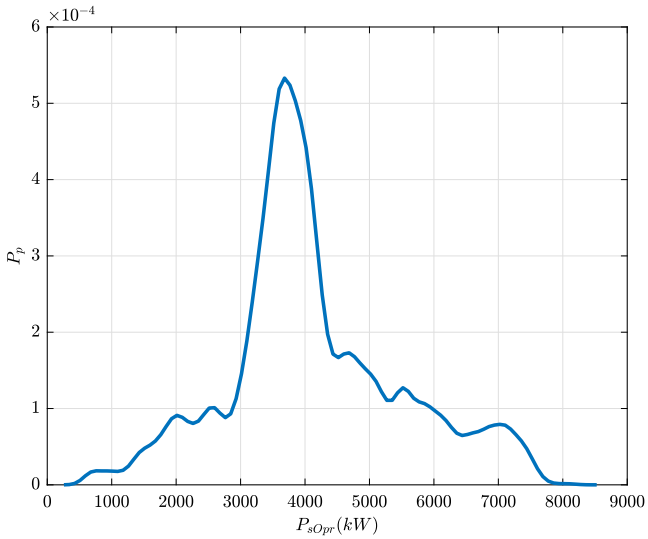

Fig. 3. Ship power profile for the studied general cargo ship.

wave periods in a grid representing a specific sea region. Based on a conditional modeling approach (CMA), a three-parameter Weibull probability density function is used to describe the significant wave height as (DNV, 2010)

$$f_{H_s}(H_s) = \frac{\beta_{H_s}}{\alpha_{H_s}}\left(\frac{H_s - \gamma_{H_s}}{\alpha_{H_s}}\right)^{\beta_{H_s}-1} \exp\left(-\frac{H_s - \gamma_{H_s}}{\alpha_{H_s}}\right)^{\beta_{H_s}} \tag{34}$$

Similarly, the peak wave period conditional on H_s is given by

$$f_{T_p|H_s}(T_p|H_s) = \frac{1}{\sigma T_p \sqrt{2\pi}} \exp\left(-\frac{(lnT_p - \mu)^2}{2\sigma^2}\right) \tag{35}$$

with

$$\mu = a_0 + a_1 H_s^{a_1} \tag{36}$$

$$\sigma = b_0 + b_1 e^{b_2 H_s} \tag{37}$$

On the basis of the data provided by DNV (2010) for different nautic zones depicted in Fig. 4, β_{H_s}, α_{H_s}, γ_{H_s}, a_m, and b_m ($m = 0, 1,$ and 2) are calculated. Then, the wave scatter diagram for any arbitrary nautic zone, SD_{wave}, is computed as follows

$$SD_{wave} = f_{H_s} \cdot f_{T_p|H_s} \tag{38}$$

The ship scatter diagram will allow us to determine the probabilities of different significant wave heights and peak wave periods encountered by the ship within her operation, $P_{SD}(H_S, T_p)$. Regarding different zones operated by the ship, the wave scatter for the overall voyage, SD_{wave}^{Voy}, is determined by

$$SD_{wave}^{Voy} = \sum_{i=1}^{n_{Zone}} P_{Zone}^{i} SD_{wave}^{i} \tag{39}$$

In this case, n_{Zone} is the number of zones contributing to the operational area and the contribution of each zone to the overall voyage is accounted for in P_{Zone}^{i}.

2.2.3. Probability of wind and wave encounter angles

To estimate the probability of the encounter wave angle, the ship in-service data of the studied ship (reference ship) is used. Furthermore, it is assumed that both waves and winds point in the same direction.

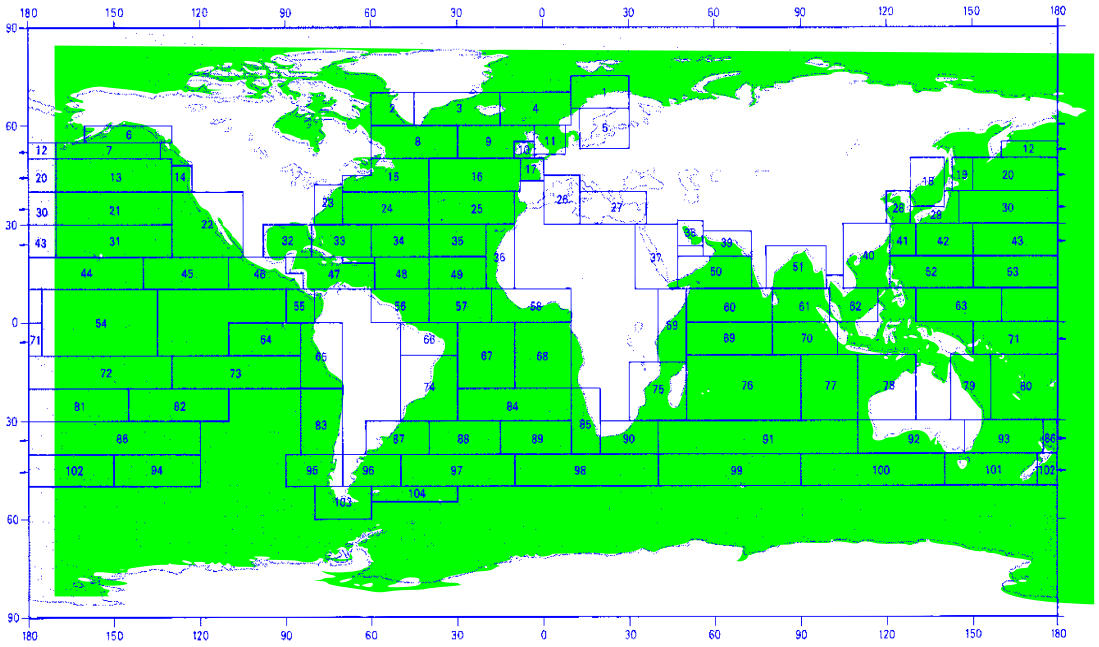

Fig. 4. Nautic zones used for estimation of long-term wave distribution parameters (DNV, 2010).

2.3. Speed-dependent constraints

To ensure the ship's long-term performance, speed-dependent constraints C_{SD}, such as engine limits, cavitation, slamming, and so on, must be checked and satisfied at each ship speed. To serve as penalty parameters in the optimization process, the speed-dependent constraints are normalized and added to the optimization objective. The engine limits and cavitation are considered in this study. However, the same procedure can be employed for other speed-dependent constraints.

2.3.1. Cavitation constraint

Cavitation might be destructive for the propeller performance by deteriorating efficiency and damaging propellers, rudders, or any other surfaces exposed to the propeller-induced cavitation. For estimating the minimum blade area ratio to avoid cavitation, Keller's criterion can be used as follows

$$A_E/A_{o_{min}} = \frac{(1.3+0.3Z)T_R}{(P_0-P_V)D_p^2} + K \tag{40}$$

For single, slow twin and fast twin-screw vessels, $K = 0.2, 0.1$, and 0, respectively.

To evaluate the cavitation on a long-term basis for sea, the penalty function for cavitation, $\bar{P}_{Cav}^{Sea}$, is expressed as

$$\bar{P}_{Cav}^{Sea} = \iiiint P_{Enc}^{tot}(\beta)\, P_{SD}(H_S,T_p)\, P_P(P_s)\, I_{Cav}(X_i,\beta,H_S,T_p,P_s)\, d\beta\, dT_p\, dH_s\, dP_s \tag{41}$$

with

$$I_{Cav}^{Sea}(X_i,\beta,H_S,T_p,P_s) = \begin{cases} 1 & A_E/A_o \le A_E/A_{o_{min}} \\ 0 & \text{otherwise.} \end{cases} \tag{42}$$

$A_E/A_{o_{min}}$ is the cavitation constraint, see Eq. (40). Also, X_i represents the decision variable vector of the optimization problem. In the same way, it can be obtained for the calm water and the design speed V_d as

$$P_{Cav}^{Calm} = I_{Cav}^{Calm}(X_i,V_d) \tag{43}$$

with

$$I_{Cav}^{Calm}(X_i,V_d) = \begin{cases} 1 & A_E/A_o \le A_E/A_{o_{min}} \\ 0 & \text{otherwise.} \end{cases} \tag{44}$$

2.3.2. Engine limit

The propeller curves over entire operating ranges are required to be within the engine load diagram defined by the engine's speed, power, mean effective pressure, and torque limits, as shown in Fig. 5. This requirement is referred to as the engine limit in this study. Here, the engine load diagram is assumed to be the same as for the parent hull. The penalty function below is used to assess the engine limit for a seaway.

$$\bar{P}_{Eng_{lim}}^{Sea} = \iiiint P_{Enc}^{tot}(\beta)\, P_{SD}(H_S,T_p)\, P_P(P_s)\, I_{Eng_{lim}}(X_i,\beta,H_S,T_p,P_s)\, d\beta\, dT_p\, dH_s\, dP_s \tag{45}$$

with

$$I_{Eng_{lim}}^{Sea}(X_i,\beta,H_S,T_p,P_s) = \begin{cases} 1 & if\ engine\ limits\ are\ not\ met \\ 0 & \text{otherwise.} \end{cases} \tag{46}$$

In the calm water and the design speed V_d, it is written as follows

$$P_{Eng_{lim}}^{Calm} = I_{Eng_{lim}}^{Calm}(X_i,V_d) \tag{47}$$

with

$$I_{Eng_{lim}}^{Calm}(X_i,V_d) = \begin{cases} 1 & if\ engine\ limits\ are\ not\ met \\ 0 & \text{otherwise.} \end{cases} \tag{48}$$

3. Optimization problem and setting

3.1. Test case

The suggested methods in Sections 2.1 and 2.2 are general and can be used for any type of ship. Here, they are tested on a general cargo ship for the preliminary design phase. The main particulars of the general cargo ship is presented in Table 1. The vessel is seven

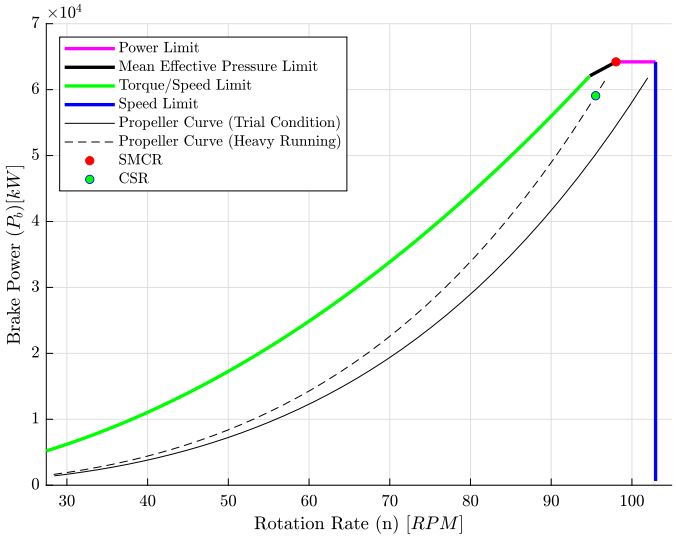

Fig. 5. Schematic engine load diagram and operating limits for a ship.

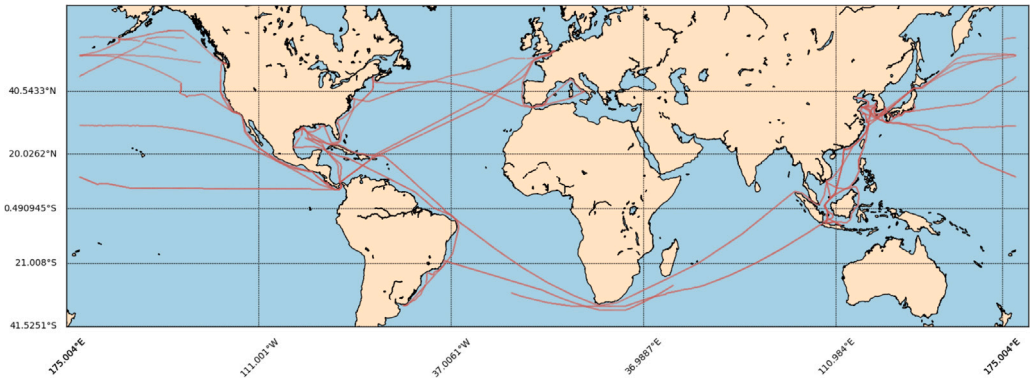

Fig. 6. The ship operational route.

Table 1
Main particulars for the studied general cargo ship.

Parameters	Value
Ship type	General cargo
Length [m]	194
Breadth [m]	32
Block coefficient [–]	0.8
Design draught [m]	12.6
Service speed [knots]	15.5

years old, and her ship-in-service data is collected over roughly her entire lifetime, through an automatic collection system with a sampling interval of 15 min. For location data, the Automatic Identification System (AIS) database is accessed, and for weather data, the European Center for Mid-range Weather Forecasts (ECMWF) database is used. In the analysis, the following parameters were examined; timestamp, shaft power, shaft speed, draft, ship speed, significant wave height, wave period, wave direction, longitude, and latitude. The probabilities of the power and the wave encounter angle are based on the in-service data of the case ship and are given in Fig. 3 and Fig. 7, respectively. The ship engine is 5S60ME-C8.5 with the engine layout diagram given in MAN (2014).

The main objective is to handle epistemic uncertainty using the method proposed in Section 2.1 and then optimize the main particulars of ship hulls and propulsion systems robust to the aleatory uncertainty in accordance with the approach outlined in Section 2.2.

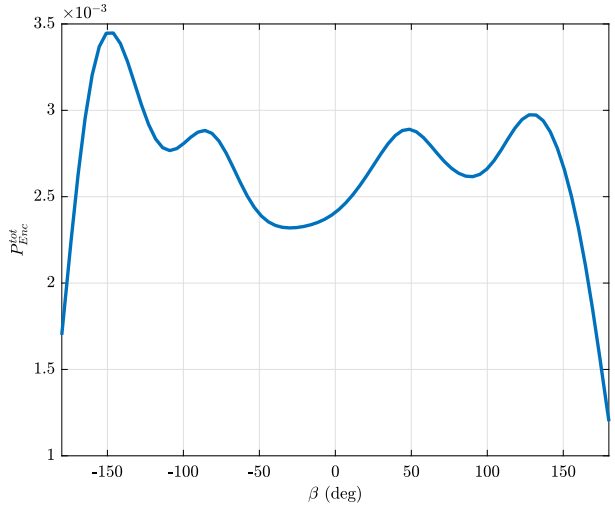

Fig. 7. Probabilities of the encounter wave angle over the entire ship voyage (0 : head wave).

3.2. Epistemic uncertainty

Here, the aim is to combine the methods discussed in Section 2.1 and obtain the optimal combination using the tuning algorithm, called

Table 2
The results of the tuning algorithms for different models.

Models	Calm water resistance	Added resistance in wave	Added resistance in wind	Propulsion system efficiency	Wetted surface area	Midship section coefficient	Waterplane area coefficient
Model 1	Holtrop–Mennen	CTH	ISO 15016	B-series	Mumford's formula	Schneekluth and Bertram	Papanikolaou
Model 2	Hollenbach	SNNM	Blendermann	B-series with ITTC full scale correction	Numerical computation	Numerical computation	Numerical computation
Model 3	Holtrop–Mennen	CTH	ISO 15016	Auf'm Keller	Numerical computation	Numerical computation	Numerical computation

Model 2. Also, by defining the optimization objective as a negative value of NRMSE, the worst combination of methods, called Model 1, is given. The results of the epistemic uncertainty analysis for the worst and the best combinations are shown in Figs. 8 and 9. It can be seen that the best method, Model 2, reached an NRMSE (in percent) of 13.44%, while the worst combination of methods, Model 1, reaches an NRMSE of 33.4%. This illustrates the effectiveness of the proposed approach in reducing epistemic uncertainties due to the model.

Furthermore, it should be noted that the accuracy of the power prediction model can be improved by adding additional parameters/methods. As an example, adding Auf'm Keller (Schneekluth and Bertram, 1998) as an alternative approach to calculate the propulsion efficiency and running the tuning approach again will result in NRMSE of only 4.8%, as presented in Fig. 10. The resulting model is referred to as Model 3. Auf'm Keller formula is written as follows

$$\eta_D = 0.885 - 0.00012 \cdot n_{rpm} \cdot \sqrt{L_{pp}} \tag{49}$$

where n_{rpm} is the propeller rpm. Nonetheless, Auf'm Keller formula does not include the design parameters of the propeller required for the ship design problem defined in this research. As a result, Model 2 will be used instead in the ship design optimization problem. Model 3 will however be applied later in Section 4.4 to evaluate the ship designed by Model 2.

The results of the power prediction models for the different models in the studied operational condition are shown in Fig. 11. The results for the models 2 and 3 indicate the high performance of the proposed approach in decreasing the inaccuracy of the model in most operational conditions. The worst model, however, shows a poorer performance in the majority of the conditions. Additionally, the comparison between the power prediction model and the ship in-service data indicates that the best power prediction models reflect the change in the power for the studied operational conditions required for the power profile-based optimization problem developed in the next section.

The details of the selected methods for the different models are provided in Table 2. The interesting point about these results is that as a result of the different input parameters and combination effects, Holtrop, CTH, and ISO 15016 are both in the category of the worst and the best models (Model 1 and Model 3) with about 86% percentage difference in the NRMSE results. These results clearly demonstrate the significant influences of the input parameters and the combination effect on the model and highlight the value of the proposed approach in improving the accuracy of the power prediction model.

3.3. Aleatory uncertainty

The previous research shows the importance of the main dimensions of the ship and propeller in a ship design optimization problem (Wang et al., 2021; Esmailian et al., 2019; Nelson et al., 2013; Esmailian et al., 2017). This research defines the main dimensions of the general cargo ship hull and propeller as the design variables and takes $\bar{V}_S^{Opt}$ as the objective function to develop an optimization problem to evaluate the performance of the approach suggested in Section 2.2. The adopted approach is general and can be used to optimize any ship type with the goal of optimizing ship energy efficiency at sea. The sizes of the ship hull and propeller are controlled through quite strict limits; 5% limit on the displacement, engine limit, intact stability requirements, cavitation, and the clearance between the ship hull and propeller as optimization constraints. Intact stability parameters and the ship displacement are calculated numerically based on the ship offset table. The cavitation and engine limits are discussed in Sections 2.3.1 and 2.3.2, respectively. A sufficient clearance between the hull and propeller is crucial in reducing vibration amplitude due to propeller excitation. Classification societies suggest a minimum geometric clearance. Here, the clearance between the propeller and the ship hull is checked by the optimization algorithm based on the values recommended by Det Norske Veritas (DNV) classification society (Papanikolaou, 2014).

It should be noted that the ship dimensions are limited by topological constraints such as canals, ports, channels, and confined waters. In this problem, the decision variable ranges satisfy the requirements of the sea regions in which the ship operates and thus there is no topological constraint in the optimization problem.

Table 3
Optimization algorithm settings.

GA Parameter	Value
Population size	40
Maximum number of generations	1000
Maximum stall generations	100
Tolerance value	0.0001
Mutation function	Constraint dependent
Selection function	Tournament

3.4. Optimization formulation and setting

The genetic algorithm (GA) is implemented using the MATLAB optimization toolbox. If the average fitness function change over generations is less than the preset tolerance, the optimal solution is reached. A new generation of design options is then generated using the GA optimization algorithm if this requirement is not met. The natural selection process eliminates individuals with lower fitness functions, leaving only those with high scores behind. The process is repeated until a suitable solution is found or the maximum number of generations has been reached. In order to reach the optimal solution, GA relies on various operators such as selection, mutation, inheritance, and recombination. The selection operator here selects members of the next generation of children based on their parental characteristics, and the crossover operator combines them to form the next generation. The mutation operator, on the other hand, applies a random change to parents. The GA settings are presented in Table 3.

The performance of the proposed strategy is evaluated with a set of cases. Case 1 represents the parent ship. Case 2 refers to the suggested optimization approach, applying the power profile and operation of the parent hull, as given in Figs. 3, 6 and 7. In recent years, we have had growing numbers of ships operating at slow steaming speeds. As a result, it is interesting to evaluate a ship design problem based on a slow steaming operational profile. Case 3 is thus defined to evaluate the effects of optimizing the ship for a different mission depicted in Fig. 12 based on a slow steaming power profile. Furthermore, Figs. 13 and 14 show the power profile and the probability of encountering waves on the new mission. A power profile similar to Case 2 and environmental conditions similar to Case 3 are used in Case 4, aiming to assess how changes in the environmental conditions of the ship affect the design. Case 5 is based on the same power profile as Case 3 and the same environmental conditions as Case 2 so as to evaluate the impacts of a change in only the power profile on the design. Case 6 reflects a traditional method in the ship design based on constant design speed in calm water, while the optimization objective is to minimize the calm

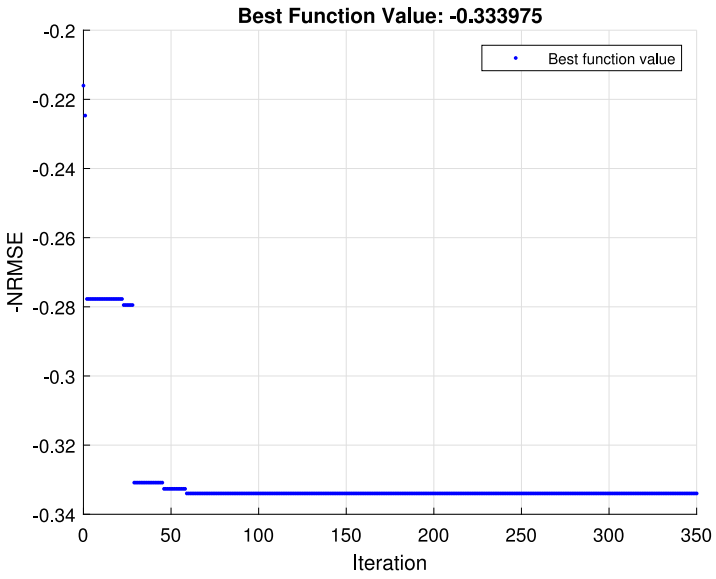

Fig. 8. Iterative convergence process of –NRMSE for Model 1.

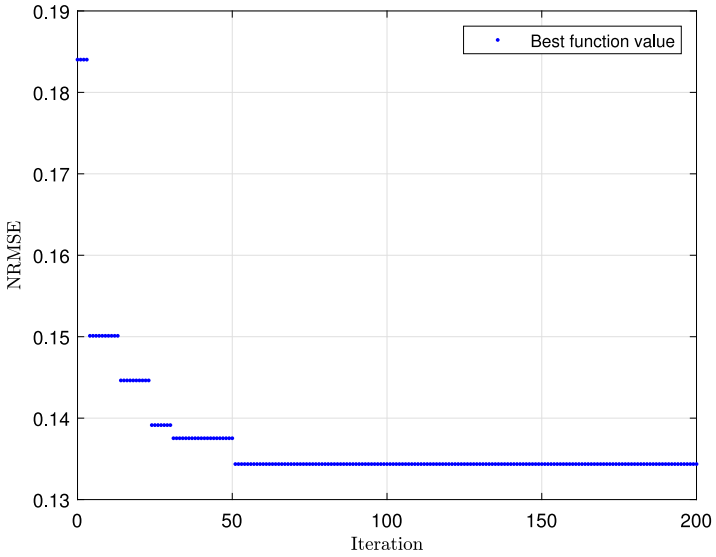

Fig. 9. Iterative convergence process of NRMSE for Model 2.

water resistance and a sea margin of $sm = 15\%$ has been assumed, which is a typical value. Defining cases 3–6 that represent design under different operational conditions, allows us to assess the effects of the aleatory uncertainties on the design. As a final case, Case 7 employs the worst power prediction model obtained in Section 3.2 (Model 1) as well as the same environmental conditions and power profile as Case 3, aiming to assess the effects of both epistemic and aleatory uncertainties on the design. Table 4 provides a brief overview of all cases.

The ship offset table for the new design is updated by scaling the ship offset table of the parent hull based on the decision variables. This is done by an automatic optimization process using the genetic optimization algorithm. Similarly, the windage dimensions of the parent ship are updated based on the decision variables. The windage dimensions for the parent hull are obtained from the general arrangement plan. Having the ship offset table, the righting lever (GZ) curve and other hydrostatic parameters are also obtained.

The vertical center of gravity over the keel, KG, is calculated by adding the vertical center of gravity above the waterline (z_G) and the draft (d), i.e., $KG = z_G + d$. Here, $z_G = KG_p - d_p = -0.1\ m$, where KG_p and d_p represent the vertical center of gravity and the draft of the parent hull, respectively. This value of z_G is applied to all ship variations.

The probabilities of exceeding the engine and cavitation limits, as the speed-dependent constraints in the optimization process, were defined in Section 2.3. To serve as penalty parameters for cavitation occurrence and exceeding the engine limit, the cavitation and engine penalty functions are added to the optimization objective. Then, the optimization objectives for cases 2–5 and 7 are expressed as

$$\bar{F}^{Sea}_{Obj} = min\ (-\bar{V}^{Opt}_{S}(X_1, \beta, H_S, T_p, P_s) + \bar{P}^{Sea}_{Eng_{lim}}(X_1, \beta, H_S, T_p, P_s) + \bar{P}^{Sea}_{Cav}(X_1, \beta, H_S, T_p, P_s)) \quad (50)$$

where $X_1 = [L_{pp}/B, B/d, L_{pp}, D_p/d, A_E/A_o, Z, P/D_p]$ represents the decision variable vector. Here, $\bar{V}^{Opt}_{S}$ is expressed in ms^{-1}. For Case 6, the optimization objective is defined as

$$\bar{F}^{Calm}_{Obj} = min\ (R^{norm}_{Calm}(X_2, V_d) + P^{Calm}_{Eng_{lim}}(X_2, V_d) + P^{Calm}_{Cav}(X_2, V_d)) \quad (51)$$

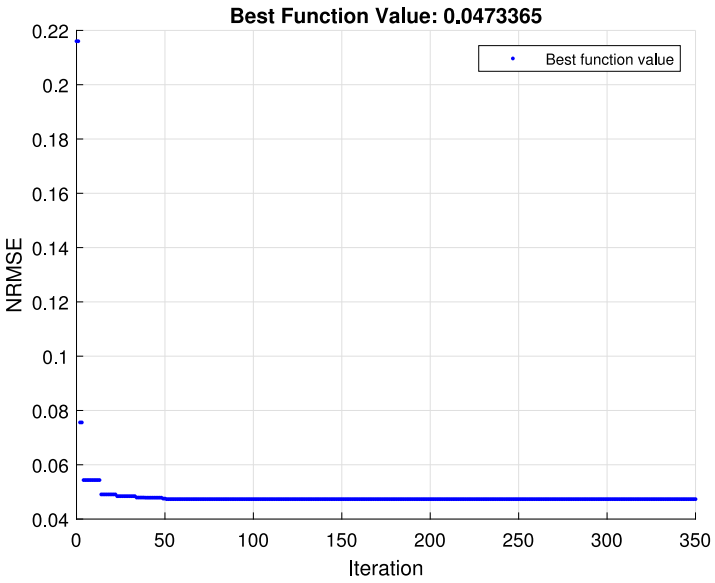

Fig. 10. Iterative convergence process of NRMSE for Model 3.

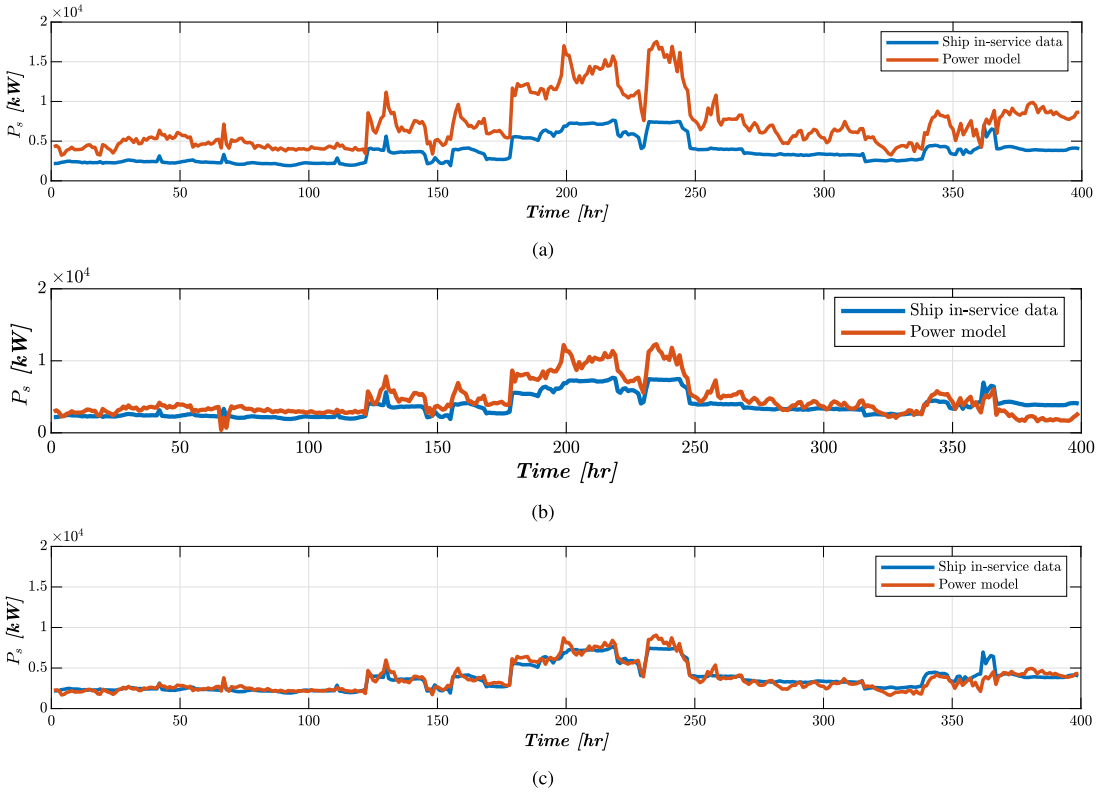

Fig. 11. The results of the power prediction model against the ship in-service data for (a) Model 1 (b) Model 2 (c) Model 3.

where $R^{norm}_{Calm}(X_2) = \frac{R_{Calm}(X_2)}{R^{init}_{Calm}}$ in which R^{init}_{Calm} is the calm water resistance for the initial (parent) hull. Also, $X_2 = [L_{pp}/B, B/d, L_{pp}]$. The details of the design problems for different cases are shown in Table 5.

4. Results and discussion

Table 6 summarizes the results of optimization problems for different cases. Note that except for cases 1 and 6, $\bar{F}_{Obj}$ in Table 6 is $\bar{F}_{Obj} = -\bar{V}^{Opt}_{S} + \bar{Pr}^{Sea}_{Eng_{lim}}/100 + \bar{Pr}^{Sea}_{Cav}/100$, evaluated using the power profile and sea environment applied in the optimization. The results show that in comparison to Case 1, all cases are more slender except for Case 6, which is designed for calm water, and they all have approximately the same block coefficient. Having a slender body might help the ships perform better at sea. Slenderness of the optimal hull (Case 2) against the parent hull is also visible in Fig. 15. It should also be taken into account that the displacement for all the optimized versions ended up at the lower limit specified (see Table 5), meaning that it is about 5% lower than the displacement of the parent. This difference

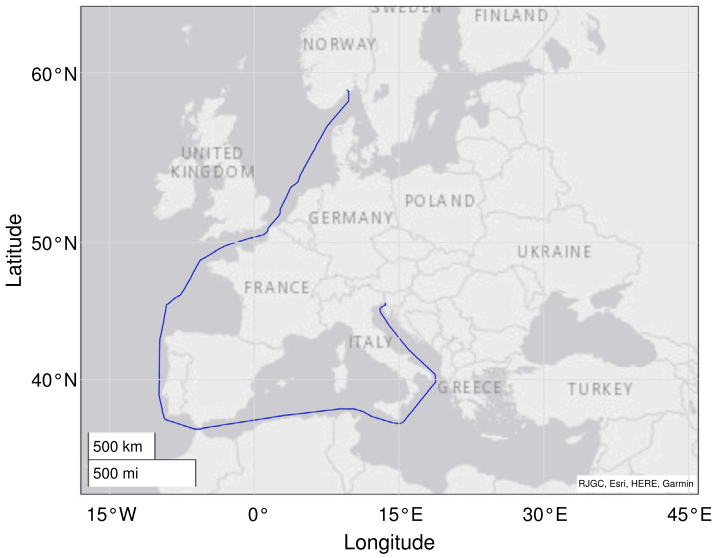

Fig. 12. A schematic of the route studied in Case 3.

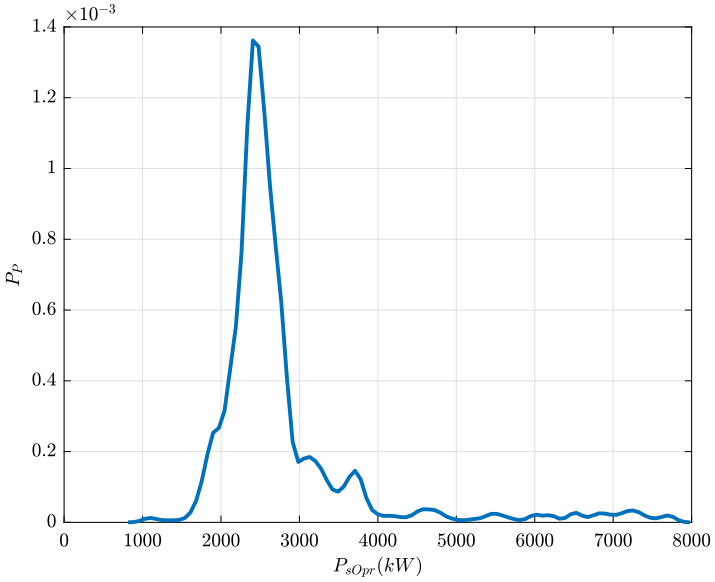

Fig. 13. Probability of the shaft power for the route studied in Case 3.

Table 4
Different cases studied in this research.

Case 1: The parent general cargo ship
Case 2: Ship design through the proposed approach in the seaway.
Case 3: Ship design through the proposed approach for a new ship mission (new power profile and environmental profile)
Case 4: Design the ship using the proposed approach for the same power profile as Case 2 and the same environmental conditions as Case 3.
Case 5: Design the ship using the proposed approach for the same power profile as Case 3 and the same environmental conditions as Case 2.
Case 6: Ship design for minimizing the ship resistance at the design speed $V_d = 15.5$ knots in the calm water condition and assuming $sm = 15\%$.
Case 7: Ship design via the proposed approach based on the worst combination of the power prediction model in the same mission as Case 3.

accounts for about 1% difference in speed, under the assumption of the constant Admiralty coefficient. The results in Table 6 show that for cases 2–5 and 7, the cavitation criterion is fulfilled ($\bar{Pr}^{Sea}_{Cav} = 0$), but they still experience a small probability of exceeding engine limits ($\bar{Pr}^{Sea}_{Eng_{lim}}$) in their studied operational conditions. The cavitation and engine limits are met by the optimization algorithm for Case 6. These results indicate that cases with different power profiles and operation profiles experience quite different average attainable speeds. To be able to compare the performance of different cases, all other results presented in the following sections are obtained using the same power profile and operational conditions that are used to optimize Case 2.

4.1. Performance in different power levels

As a supplement to evaluate the performance of the different cases with given power profiles, it is of interest to see how they perform at a range of constant power levels. This is done by selecting a set of powers between 1350 kW and 7700 kW that fall within the ship's power profile range. In order to obtain the corresponding parameters for different powers, a method similar to that presented in Fig. 2 and Section 2.2 is applied. The results are shown in Fig. 16. Different parameters presented in Fig. 16 are averaged over the long term for the

Table 5
Decision variable ranges, constraints, and optimization objectives of different cases.

	Cases 2–5 and Case 7	Case 6
Decision variables	$5.0 \le L_{pp}/B \le 8.0$ $2.0 \le B/d \le 3$ $180 \le L_{pp}[\text{m}] \le 210$ $0.5 \le D_p/d \le 0.7$ $0.55 \le A_E/A_o \le 1.05$ $4 \le Z \le 6$ $0.5 \le P/D_p \le 1.4$	$5.0 \le L_{pp}/B \le 8.0$ $2.0 \le B/d \le 3.0$ $180 \le L_{pp}[\text{m}] \le 210$
Subject to	$\lvert\frac{\Delta-\Delta_0}{\Delta_0}\rvert \le 0.05$ $GZ\ area$ (0–30 deg) ≥ 0.055 m rad $GZ\ area$ (0–40 deg) ≥ 0.09 m rad $GZ\ area$ (30–40 deg) ≥ 0.03 m rad $GM \ge 0.15$ m $Angle\ at\ GZmax \ge 30$ deg $GZ_{max} \ge 0.2$ m Clearance limits (Papanikolaou, 2014)	$\lvert\frac{\Delta-\Delta_0}{\Delta_0}\rvert \le 0.05$ $0.5 \le D_p/d \le 0.7$ $GZ\ area$ (0–30 deg) ≥ 0.055 m rad $GZ\ area$ (0–40 deg) ≥ 0.09 m rad $GZ\ area$ (30–40 deg) ≥ 0.03 m rad $GM \ge 0.15$ m $Angle\ at\ GZmax \ge 30$ deg $GZ_{max} \ge 0.2$ m Clearance limits (Papanikolaou, 2014)
Optimization objective	$\bar{F}_{Obj}^{Sea}$	$\bar{F}_{Obj}^{Calm}$

Table 6
Decision variables and objectives for different cases.

Decision variables	Case 1	Case 2	Case 3	Case 4	Case 5	Case 6	Case 7
L_{pp} [m]	194	207.32	206.96	207.33	205.00	193.50	201.32
B [m]	32	30.44	30.53	30.51	30.56	31.29	32.43
d [m]	12.6	11.88	11.86	11.85	11.95	12.31	11.53
D_p [m]	7	7.34	7.61	7.23	7.66	7	7
EAR	0.540	0.561	0.572	0.585	0.580	0.540	0.635
Z	4	4	4	4	4	4	5
P/D_p	0.79	0.69	0.71	0.71	0.70	0.79	0.79
Δ [t]	6.36E+04	6.04E+04	6.04E+04	6.04E+04	6.04E+04	6.04E+04	6.04E+04
C_B	0.80	0.79	0.79	0.79	0.79	0.80	0.79
S_{wet} [m^2]	9.529E+03	9.558E+03	9.551E+03	9.559E+03	9.510E+03	9.260E+03	9.435E+03
$\bar{F}_{Obj}$	–	−5.41	−4.48	−5.37	−4.43	0.95	−3.69
$\bar{Pr}_{Eng_{lim}}^{Sea}$ [%][a]	–	1.82	3.14	2.13	0.85	–	1.75
$\bar{Pr}_{Cav}^{Sea}$ [%]	–	0	0	0	0	–	0
$\bar{V}_S^{Opt}$ [ms^{-1}]	–	5.43	4.51	5.39	4.44	–	3.71

$\bar{Pr}_x^y = \bar{P}_x^y \times 100$

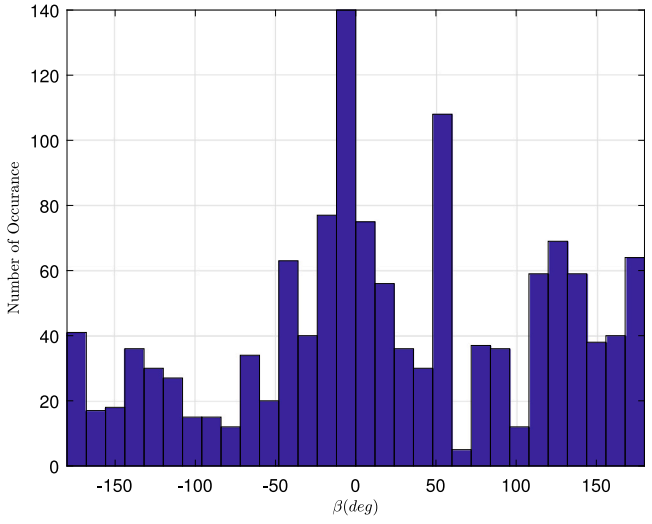

Fig. 14. Probability of the encounter wave angle for the route studied in Case 3.

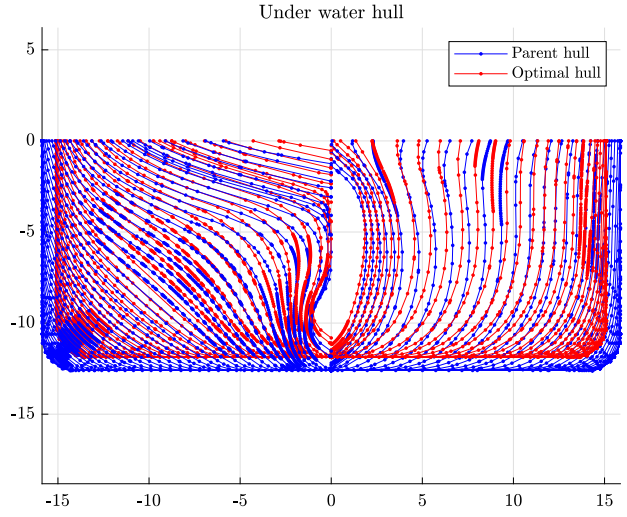

Fig. 15. Comparison of ship under water hull for the optimal hull against parent hull.

same environmental parameters as Case 2. This means that the power profile is replaced by a set of constant powers, so that each power level results in one average speed for each ship case, evaluated over the complete operational profile of Case 2. Based on these results, it appears that the performance of different cases varies with power, and the higher the power, the greater the difference between cases.

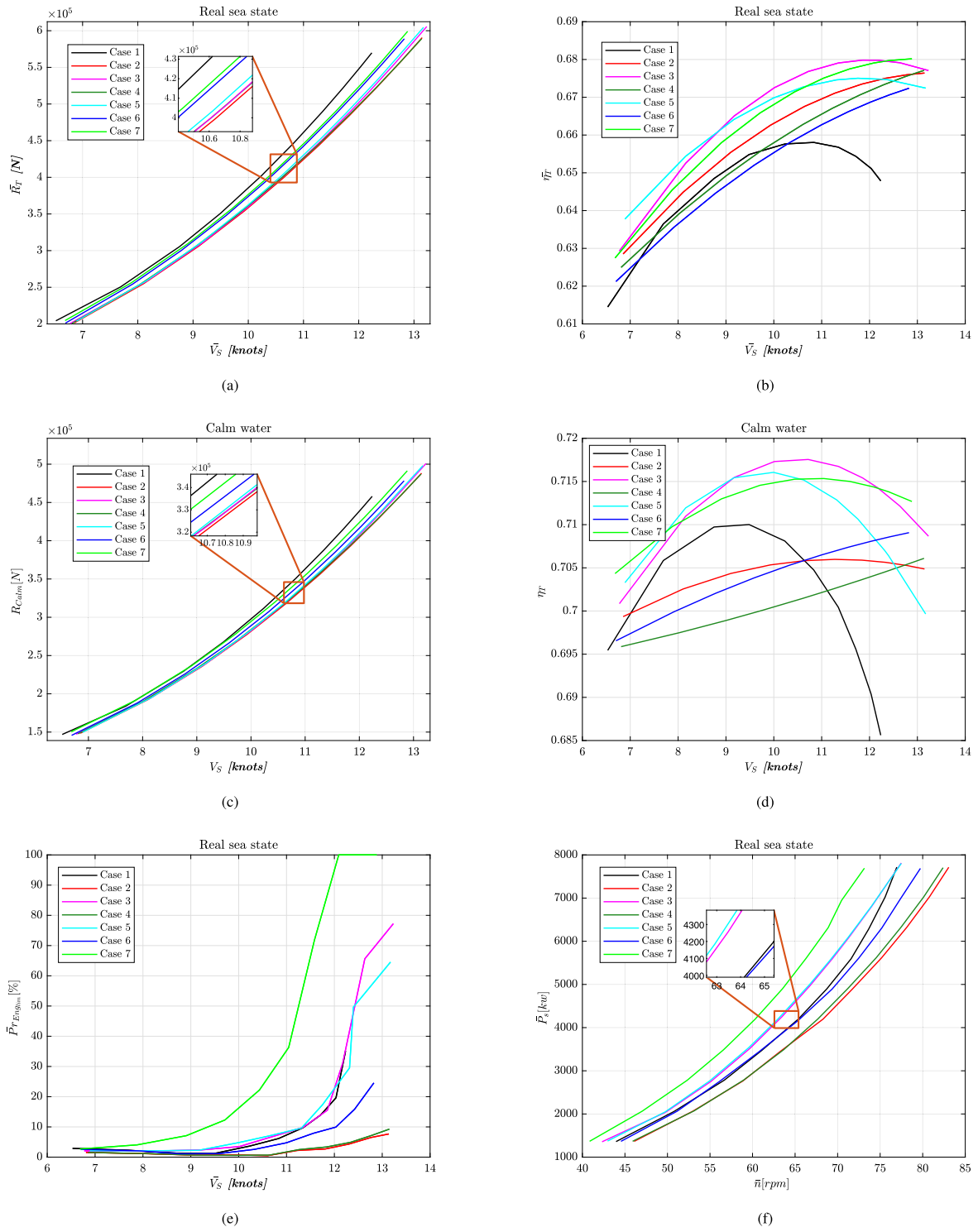

Fig. 16. Performance of the different cases evaluated over the long term at a range of constant power levels. The environmental profile applied is the one used to optimize Case 2.

It can be seen from Fig. 16(c) that Case 6 (defined to minimize the calm water resistance) experiences lower average calm water resistance than the parent hull, but her resistance is slightly higher than Case 2. The reason is that some design constraints in the optimization problem are influenced by both hull and propeller parameters, such as the cavitation and engine limits. In Case 6, those constraints can only be met by changing the hull parameters while the propeller parameters are fixed. In Case 2, both propeller and hull parameters can be changed to meet those constraints. Therefore, the hull parameters in Case 2 are more flexible than those in Case 6. This has resulted in finding better results for calm water resistance in Case 2 than in Case 6.

The probabilities of exceeding engine limits have increased with ship speed, as shown in Fig. 16(e). In addition, Fig. 16(e) shows that cases 6 and 7 have experienced higher levels of engine limit exceeding despite their higher efficiency and lower resistance. The reason is that the average required propeller revolution to reach a given power for those cases is lower than in other cases, as can be seen from Fig. 16(f). The ability of an engine to provide torque for a given engine

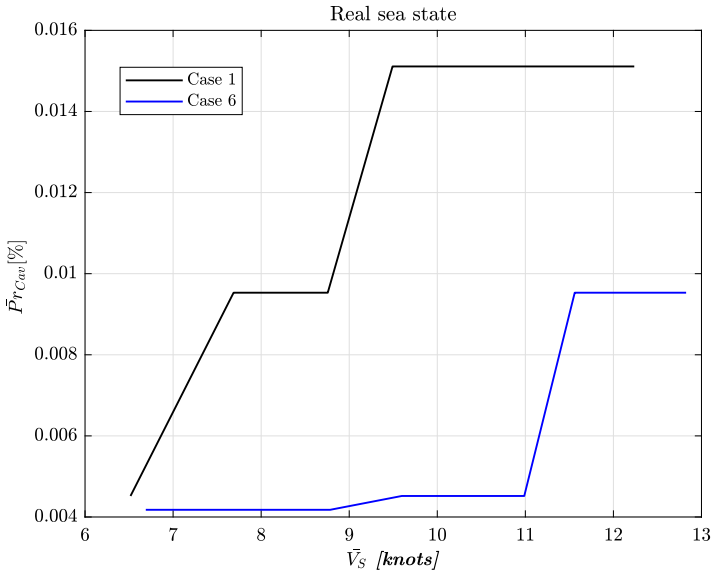

Fig. 17. The average probability of occurring the cavitation over the long term against the average attainable ship speed in real sea state for cases 1 and 6. The results for other cases are zero.

power is reduced by reducing the propeller revolutions. As a result, the probability of exceeding the engine limits increases. The probability of exceeding the engine limits for the parent hull (Case 1) is also high, as shown in Fig. 16(e). The reason is that the parent hull experiences high resistance and low efficiency in most of the operating range, as can be seen in Figs. 16(a) and 16(b). As compared with other cases, cases 2 and 4, designed based on the ship's actual power profile, experience lower probabilities of exceeding the engine limits than other cases. Moreover, the results for Case 6 indicate that design in calm water with the sea margin of 15% has reduced the probability of exceeding the engine limits compared to the parent hull, but it is still high compared to cases 2 and 4.

Overall, these results imply the importance of matching the engine and the propeller throughout the range of operation to ensure that the engine torque and propeller torque do not overload the engine and that the thrust needed to reach desired speeds is available over the entire operating range.

4.2. Effects of exceeding engine limits on the attainable speed

Due to exceeding the engine limits, the ship speed will be reduced to a certain level based on the captain's decision. Here, it is assumed that once the engine limits are exceeded, the captain would slow down the ship speed until the engine limits are met. On the basis of this assumption and the same power profile and environment used to optimize Case 2, the average attainable ship speed denoted by $\bar{V}_S^{RSS}$ is obtained. The results for different cases are presented in Table 7. The results presented in Table 8 indicate the percentage change (PC) of the average attainable ship speed $\bar{V}_S^{RSS}$ for different cases. Accordingly, 7.15%, 7.78%, 1.73%, 7.73%, 4.77% and 26.91% reductions in the average ship speed $\bar{V}_S^{RSS}$ in cases 1, 3, 4, 5, 6, and 7 compared to Case 2 have been found, implying the effectiveness of the proposed approach in the optimal design of a ship at real sea states. When comparing the results of the average attainable speed $\bar{V}_S^{RSS}$ of Case 2 with cases 3, 4, and 5, it can be seen that the design of ships with different power profiles and environmental conditions negatively impacts the results. In addition, as compared to cases 3 and 5, Case 4 has an average attainable speed of 10.21 knots, which is closer to the optimum hull (Case 2), suggesting that the power profile has a higher impact on the studied ship design problem than environmental conditions. Further, comparing Case 7 with Case 2 reveals that the average achievable speed has been reduced by 26.91%, suggesting that the epistemic and aleatory uncertainties have led to suboptimal designs. It might be argued that the performance of Case 7 should be evaluated using the same power prediction method that is used to optimize it. That is provided by $\bar{V}_S^{Opt}$ in Table 6, corresponding to an average speed of 7.21 knots.

It can be seen from Table 7 that both Case 3 and Case 5 achieve a lower average speed than the parent hull (Case 1). This indicates that it is important that the actual power profile and sea environment are applied in the optimization of the proposed method to give better designs. In addition, it can be found from Fig. 16(e) that a ship optimized based on a slow steaming operational profile might experience a significant voluntary speed loss over the long term due to exceeding engine limits if she operates at higher speeds.

It is seen from Table 7 that Case 3 gives a lower average speed than Case 1. The reason is that Case 3 is optimized for a different power and operational profile than that used for computing the average speed in Table 7. Therefore, we have computed the average speed of Case 1 using the power profile (Fig. 13) and environmental operational condition of Case 3, which gave an average speed of 8.25 knots, which is still lower than the comparable average speed of Case 3, which is given in Table 6 as $\bar{V}_S^{Opt} = 4.51$ ms^{-1}, corresponding to 8.77 knots. Thus, the suggested optimization procedure also works for this alternative power and operational profile, although the gain is smaller, perhaps due to the low powers dominating the power profile of Case 3. In this connection, it is worth noting that the average speed of Case 2 evaluated using the power and operational profile of Case 3 is 8.64 knots, which is lower than the 8.77 knots obtained by Case 3 for the same operation. Moreover, since Case 7 is optimized using the same power and operational profile as Case 3, 7.21 knots achieved by Case 7 is comparable with the 8.77 knots resulted from Case 3 in the same conditions, indicating that it is important to use the best possible power prediction method in the optimization.

In the conceptual phase of ship design, estimating the ship building cost is a big challenge. However, to make a shipbuilding contract successful, a fair estimation of the cost is necessary (Ross, 2004). An empirical formula obtained through statistical regression analysis can be applied in this context. There are a number of empirical formulas

Table 7
The average attainable ship speed $\bar{V}_S^{RSS}$ for different cases when taking the engine limits into account. The environmental profile applied is the one used to optimize Case 2.

	Case 1	Case 2	Case 3	Case 4	Case 5	Case 6	Case 7
$\bar{V}_S^{RSS}$[knots]	9.65	10.39	9.58	10.21	9.59	9.90	7.60

Table 8
Percentage change (PC) of the average attainable ship speed $\bar{V}_S^{RSS}$ for different cases.

	PC_{21} [a]	PC_{23}	PC_{24}	PC_{25}	PC_{26}	PC_{27}
$\bar{V}_S^{RSS}$	−7.15	−7.78	−1.73	−7.73	−4.77	−26.91

[a] $PC_{ij} = \frac{Objective_j - Objective_i}{Objective_i} \times 100$.

proposed in Miroyannis (2006) for estimating ship costs during the concept, preliminary, and contract design stages. Based on those formulas, if the ship type, displacement, and shipyard are the same, the ship construction costs could be assumed to be the same at the preliminary phase of the design. In this study, the displacement is constrained to be within only up to 5% of that of the parent hull. As a result, the effects of the ship building costs are ignored, and only the operational cost due to fuel consumption is considered in order to examine the cost effectiveness. In this way, it is assumed that the cost effectiveness depends on the energy efficiency of the ship over the entire operating range, making Case 2 the most cost-effective option.

Overall, cases 2 and 4 experience lower voluntary and involuntary speed losses at sea, but Case 2 is slightly better. On the other side, cases 3, 5, and 7, which were developed in order to evaluate the effects of uncertainties on the design, do not perform that well at sea.

4.3. Principle particulars of propeller

The diameter of a propeller plays an important role in propeller performance; a larger propeller diameter generally results in higher propeller efficiency. However, the diameter behind the ship is limited by the vessel draught and the required gap between the propeller and the hull to minimize vibration. In addition, there is a very close correlation between the shaft speed and the diameter of the propeller. From an efficiency perspective, a shaft with a low speed is ideal. However, this results in higher shaft torques and consequently larger shafts. As a result, it is necessary to strike a balance when designing the propeller in order to make it perform well. A propeller design optimization is helpful to meet the balance. Table 6 shows that cases 2–4 have reached a slightly larger diameter than Case 1, resulting in a positive impact on the propulsion system efficiency.

In order to optimize propeller performance for a given propeller diameter, it is necessary to find the optimum pitch ratio. The effect of pitch ratio on propeller efficiency is also strongly influenced by the ship speed and the propeller load. In this way, designing a ship based on her operational profile can result in propellers with better performance at different speeds and loads. Based on Table 6, except for cases 6 and 7, other cases have lower pitch ratios than Case 1.

In order to attain maximum efficiency, the expanded area ratio needs to be as small as possible while being high enough to prevent the cavitation. In Table 6, except for Case 6, others have a greater expanded aspect ratio than the parent hull (Case 1), resulting in a positive impact on cavitation avoidance. Fig. 17 has been obtained along with the results presented in Fig. 16. Fig. 17 shows that the probability of cavitation occurrence in all cases other than cases 1 and 6 is zero. However, cases 1 and 6 have still a small probability of the cavitation occurrence.

4.4. Short-term analysis

The previous results showed that the proposed approach has led to a better ship design evaluated on a long-term basis. To further evaluate the performance of the proposed approach, a short-term evaluation is conducted in this section. Like Section 3.1, the ECMWF weather data is used rather than the scatter diagram applied in the optimization problem. In addition, Model 3 presented in Section 3.2 is employed, which showed lower epistemic uncertainty than the power prediction model used in the optimization problem (Model 2). The short-term analysis of the optimal hull against the parent hull can be seen in Fig. 18. In-service data are used to obtain the speed of the parent ship. The results indicate that the performance of the ships varies depending on operational conditions, while the optimal hull shows better performance in general. In the light of employing a different weather database and power prediction model than those used in the optimization problem, these results reaffirm the robustness of the suggested approach in the presence of both epistemic and aleatory uncertainties.

5. Conclusion

This paper suggests a two-stage approach for the optimization of ships in real sea states under both aleatory and epistemic uncertainties associated with the weather and power prediction model. Accordingly, to reduce the epistemic uncertainties, a tuning technique based on comparing the results of the power prediction model and ship-in service data for a reference vessel (or parent hull) is developed. To reduce aleatory uncertainties due to the weather, a probability-based optimization method is suggested. It is done by defining the ship power profile and environmental characteristics as probability variables and the average attainable ship speed over the long term as the optimization objective. As a test case, a general cargo ship is used, aiming to optimize the main dimensions of the ship and propeller considering the engine limits, intact stability requirements, cavitation, clearance limits between the hull and propeller, and the displacement as the optimization constraints. The proposed approach is compared with a set of design cases representing different ship design approaches. A short-term analysis is also conducted to further evaluate the performance of the suggested approach in the presence of the aleatory and epistemic uncertainties. Analysis of the epistemic uncertainties results in up to 86% improvement in the accuracy of the power prediction model using the suggested method. In addition, the results indicate a strong influence of the input parameters and the method combination in providing an accurate power prediction model, placing Holtrop–Mennen, CTH, and ISO 15016 in the category of both worst and best power prediction models. As there is a growing interest in the number of studies applying the ship in-service data for verification and prediction purposes, the use of the proposed tuning approach to reduce the epistemic uncertainties and provide more reliable results is recommended.

The results of the probability-based ship design optimization problem show that the optimized hulls became more slender compared to the parent hull. Furthermore, the results show that there can be a significant difference in average attainable speed using the proposed approach (Case 2) when compared to other cases. The results for Case 7, which is optimized in the presence of epistemic and aleatory uncertainties, show a 26.91% reduction in the average achievable speed and a considerably higher probability of exceeding the engine limits than the optimal case. The results also indicate that with the proposed

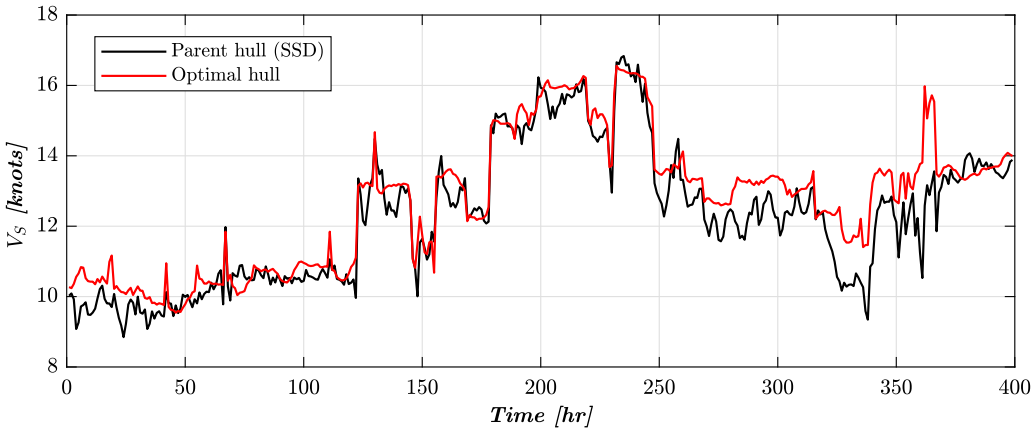

Fig. 18. Comparison of the attainable ship speed across different cases.

approach, failure of the engine limits and the resulting voluntary speed losses can be handled better than assuming the sea margin of 15%, which is a typical value. It is also reported that optimizing a ship based on the slow steaming operational profile might negatively affect the ship performance at higher speeds.

According to the results, the optimal hull has a larger propeller diameter and EAR, but a lower pitch ratio than the parent hull, enabling her to meet the design requirements and perform better across the entire operating range. Moreover, the results of the study reveal that changes in the power profile and environmental conditions might have a significant influence on the optimized design, meaning that it is important to carefully select power profile and environmental conditions to be used in such optimization problems.

A short-term analysis involving a different power prediction model and environmental parameter sources than for the design problem is conducted, aiming to further assess the performance of the proposed approach in the presence of the aleatory and epistemic uncertainties. The results reaffirm that the ship designed based on the proposed approach keeps her high performance.

In total, the results suggest that the proposed approach is effective in the design of ships for real sea states in the presence of aleatory arising from the ship's unpredictable weather and epistemic uncertainties associated with the model. For future studies, it would be interesting to evaluate the performance of the proposed approaches in other ship types and application scenarios. Since it is found that the power prediction model is of significant importance for the optimized ship design, developing improved power prediction models, that still have acceptable computational expense should be pursued.

In this study, the main purpose was to evaluate the potential of the proposed method in improving the energy efficiency of ships at sea. However, by defining a multi-objective optimization problem, the suggested method can be expanded to include cargo capacity requirements, building costs, logistics, etc., resulting in a holistically optimized design.

The results of the probability-based ship design optimization show that the performance of the ship might be improved by optimizing the design for the actual operation, including the environment in the area of the operation. This raises new challenges since the designer and the prospective operator must select which trade to design the ship for. More work might be needed to find good strategies for this selection. Furthermore, it is also found that the power prediction method to be applied in the design optimization can be significantly improved by tuning against known performance data. This means that the designer will need access to performance data, for instance from operations of similar ships operating in a similar trade, in order to tune the method in each case.

CRediT authorship contribution statement

Ehsan Esmailian: Conceptualization, Investigation, Methodology, Software, Writing – original draft. **Sverre Steen:** Conceptualization, Writing – review & editing, Methodology, Supervision. **Kourosh Koushan:** Review & editing, Supervision.

Declaration of competing interest

The authors declare that they have no known competing financial interests or personal relationships that could have appeared to influence the work reported in this paper.

Data availability

The authors do not have permission to share data.

Acknowledgment

The research was conducted at SFI Smart Maritime (WP2), funded by the Research Council of Norway (Grant number 237917), under the Center for Research-based Innovation (SFI) scheme.

References

Blendermann, W., 1995. Estimation of wind loads on ships in wind with a strong gradient. In: OMAE, vol. 1. pp. 271–277.

Chen, X., Diez, M., Kandasamy, M., Zhang, Z., Campana, E.F., Stern, F., 2015. High-fidelity global optimization of shape design by dimensionality reduction, metamodels and deterministic particle swarm. Eng. Optim. 47 (4), 473–494.

Clausen, H.B., Friis-Hansen, A., Bjø rneboe, N., et al., 2001. Bayesian and neural networks for preliminary ship design. Mar. Technol. SNAME News 38 (04), 268–277.

Coppedè, A., Gaggero, S., Vernengo, G., Villa, D., 2019. Hydrodynamic shape optimization by high fidelity CFD solver and Gaussian process based response surface method. Appl. Ocean Res. 90, 101841.

D'Agostino, D., Serani, A., Diez, M., 2020. Design-space assessment and dimensionality reduction: An off-line method for shape reparameterization in simulation-based optimization. Ocean Eng. 197, 106852.

Diez, M., He, W., Campana, E.F., Stern, F., 2014. Uncertainty quantification of Delft catamaran resistance, sinkage and trim for variable Froude number and geometry using metamodels, quadrature and Karhunen–Loève expansion. J. Mar. Sci. Technol. 19 (2), 143–169.

Diez, M., Peri, D., Campana, E.F., Iemma, U., 2010. Robust decision making in aerial and marine vehicles optimization: a designer's viewpoint. Enterprise Risk Manag. 2 (1), 68.

DNV, 2010. DNV-RP-c205: environmental conditions and environmental loads. DNV, Norway.

Esmailian, E., Ghassemi, H., Zakerdoost, H., 2017. Systematic probabilistic design methodology for simultaneously optimizing the ship hull–propeller system. Int. J. Naval Archit. Ocean Eng. 9 (3), 246–255.

Esmailian, E., Gholami, H., Røstvik, H.N., Menhaj, M.B., 2019. A novel method for optimal performance of ships by simultaneous optimisation of hull-propulsion-BIPV systems. Energy Convers. Manage. 197, 111879.
Esmailian, E., Kim, Y., Steen, S., Koushan, K., 2022. A new power prediction method toward efficient ship design and operation. Available at SSRN 4272390.
Esmailian, E., Steen, S., 2022. A new method for optimal ship design in real sea states using the ship power profile. Ocean Eng. 259, 111893.
Hang Hou, Y., jia Li, Y., Liang, X., 2019. Mixed aleatory/epistemic uncertainty analysis and optimization for minimum EEDI hull form design. Ocean Eng. 172, 308–315.
Hannapel, S., Vlahopoulos, N., 2010. Introducing uncertainty in multidiscipline ship design. Naval Eng. J. 122 (2), 41–52.
Hollenbach, K.U., 1998. Estimating resistance and propulsion for single-screw and twin-screw ships-ship technology research 45 (1998). Schiffstechnik 45 (2), 72.
Holtrop, J., 1984. A statistical re-analysis of resistance and propulsion data. Int. Shipbuild. Prog. 31 (363), 272–276.
Hou, Y., Xiong, Y., Zhang, Y., Liang, X., Su, L., 2021a. Vessel energy efficiency uncertainty optimization analysis in ice zone considering interval parameters. Ocean Eng. 232, 109114.
Hou, Y., Xiong, Y., Zhang, Y., Liang, X., Su, L., 2021b. Vessel energy efficiency uncertainty optimization analysis in ice zone considering interval parameters. Ocean Eng. 232, 109114.
ISO, 2015. ISO 15016:2015-Ships and marine technology — Guidelines for the assessment of speed and power performance by analysis of speed trial data. ISO, Geneva, Switzerland.
ITTC, 2014. 1978 ITTC performance prediction method. Recommended Procedures and Guidelines.
Kim, Y.-R., Esmailian, E., Steen, S., 2022. A meta-model for added resistance in waves. Ocean Eng. (ISSN: 0029-8018) 266, 112749.
Koushan, K., et al., 2007. Dynamics of propeller blade and duct loading on ventilated thrusters in dynamic positioning mode. In: DP Conference. pp. 1–13.
Kramer, M., Motley, M., Young, Y., 2010. Probabilistic-based design of waterjet propulsors for surface effect ships. In: Proceedings of the 29th American Towing Tank Conference. ATTC.
Kristensen, H.O., Lützen, M., 2012. Prediction of resistance and propulsion power of ships. Clean Ship. Currents 1 (6), 1–52.
Kristensen, H.O., Lützen, M., Bingham, H.B., 2017. Prediction of resistance and propulsion power of ships (Work Package 2, Report no. 4). Technical Report, Technical University of Denmark.
Lang, X., Mao, W., 2021. A practical speed loss prediction model at arbitrary wave heading for ship voyage optimization. J. Mar. Sci. Appl. 20 (3), 410–425.
Leotardi, C., Campana, E.F., Diez, M., 2015. On the use of uncertainty quantification in variable-accuracy simulation-based multidisciplinary optimization. In: 3rd Workshop on Uncertainty Quantification in Computational Fluid Dynamics.
Li, S., Benson, S., et al., 2021. A probabilistic approach to assess the computational uncertainty of ultimate strength of hull girders. Reliab. Eng. Syst. Saf. 213, 107688.
Liu, S., Papanikolaou, A., 2020. Regression analysis of experimental data for added resistance in waves of arbitrary heading and development of a semi-empirical formula. Ocean Eng. 206, 107357.
MAN, 2014. MAN B&W S60ME-C8.2-TII—Project guide—Electronically controlled two-stroke.
MathWorks, 2022. Surrogate optimization for global minimization of time-consuming objective functions. https://es.mathworks.com/help/gads/surrogateopt.html. (Accessed 04 May 2022).
McCarthy, J.H., 1961. On the calculation of thrust and torque fluctuations of propellers in nonuniform wake flow. Technical Report, DAVID TAYLOR MODEL BASIN WASHINGTON DC.
Miroyannis, A., 2006. Estimation of ship construction costs (Ph.D. thesis). Massachusetts Institute of Technology.
Motley, M.R., Nelson, M., Young, Y.L., 2012. Integrated probabilistic design of marine propulsors to minimize lifetime fuel consumption. Ocean Eng. 45, 1–8.
Motley, M.R., Young, Y.L., 2011. Performance-based design and analysis of flexible composite propulsors. J. Fluids Struct. 27 (8), 1310–1325.
Nelson, M., Temple, D., Hwang, J.T., Young, Y.L., Martins, J., Collette, M., 2013. Simultaneous optimization of propeller–hull systems to minimize lifetime fuel consumption. Appl. Ocean Res. 43, 46–52.
Nikolopoulos, L., Boulougouris, E., 2018. A methodology for the holistic, simulation driven ship design optimization under uncertainty. In: Marine Design XIII, Volume 1: Proceedings of the 13th International Marine Design Conference (IMDC 2018), June 10-14, 2018, Helsinki, Finland. CRC Press, p. 227.
Nikolopoulos, L., Boulougouris, E., 2020. A novel method for the holistic, simulation driven ship design optimization under uncertainty in the big data era. Ocean Eng. 218, 107634.
Oosterveld, M.W.C., van Oossanen, P., 1975. Further computer-analyzed data of the Wageningen B-screw series. Int. Shipbuild. Prog. 22 (251), 251–262.
Papanikolaou, A., 2014. Ship Design: Methodologies of Preliminary Design. Springer.
Perez, T., Smogeli, O., Fossen, T., Sorensen, A., 2006. An overview of the marine systems simulator (MSS): A simulink toolbox for marine control systems. Model. Identif. Control 27 (4), 259–275.
Priftis, A., Boulougouris, E., Turan, O., Atzampos, G., 2020. Multi-objective robust early stage ship design optimisation under uncertainty utilising surrogate models. Ocean Eng. 197, 106850.
Radan, D., 2008. Integrated control of marine electrical power systems.
Ralph, F.E., 2016. Design of ships and offshore structures: a probabilistic approach for multi-year ice and iceberg impact loads for decision-making with uncertainty (Ph.D. thesis). Memorial University of Newfoundland.
Ren, J., Lützen, M., 2015. Fuzzy multi-criteria decision-making method for technology selection for emissions reduction from shipping under uncertainties. Transp. Res. D Transp. Environ. 40, 43–60.
Resolution, M., 2018. 304 (72) Initial IMO strategy on reduction of GHG emissions from ships. MEPC 72, 17.
Ross, J.M., 2004. A practical approach for ship construction cost estimating. In: COMPIT'04. Citeseer.
Schneekluth, H., Bertram, V., 1998. Ship Design for Efficiency and Economy, vol. 218. Butterworth-Heinemann Oxford.
Serani, A., Diez, M., 2018. Shape optimization under stochastic conditions by design-space augmented dimensionality reduction. In: 2018 Multidisciplinary Analysis and Optimization Conference. p. 3416.
Serani, A., Diez, M., Wackers, J., Visonneau, M., Stern, F., 2019. Stochastic shape optimization via design-space augmented dimensionality reduction and rans computations. In: AIAA SciTech 2019 Forum. p. 2218.
Smith, T.W., Jalkanen, J., Anderson, B., Corbett, J., Faber, J., Hanayama, S., O'keeffe, E., Parker, S., Johansson, L., Aldous, L., et al., 2015. Third IMO greenhouse gas study 2014.
Smogeli, Ø.N., 2006. Control of marine propellers: from normal to extreme conditions.
Smogeli, Ø.N., Sørensen, A.J., 2009. Antispin thruster control for ships. IEEE Trans. Control Syst. Technol. 17 (6), 1362–1375.
Sørensen, A.J., Smogeli, Ø.N., 2009. Torque and power control of electrically driven marine propellers. Control Eng. Pract. 17 (9), 1053–1064.
Stewart, R.H., 2008. Introduction to Physical Oceanography. Department of Oceanography, Texas A and M University.
Temple, D., Collette, M., 2012. Multi-objective hull form optimization to compare build cost and lifetime fuel consumption. In: International Marine Design Conference, IMDC, Glasgow, Scotland. pp. 11–14.
Tillig, F., Ringsberg, J.W., Mao, W., Ramne, B., 2018. Analysis of uncertainties in the prediction of ships' fuel consumption–from early design to operation conditions. Ships Offshore Struct. 13 (sup1), 13–24.
Wang, H., Hou, Y., Xiong, Y., Liang, X., 2021. Research on multi-interval coupling optimization of ship main dimensions for minimum EEDI. Ocean Eng. 237, 109588.
Wei, X., Chang, H., Feng, B., Liu, Z., Huang, C., 2019. Hull form reliability-based robust design optimization combining polynomial chaos expansion and maximum entropy method. Appl. Ocean Res. 90, 101860.
Wei, H., Matteo, D., Campana, E.F., Stern, F., Zou, Z.-j., 2013. A one-dimensional polynomial chaos method in CFD–based uncertainty quanti-fication for ship hydrodynamic performance. J. Hydrodyn. Ser. B 25 (5), 655–662.
Xuan, H., Liu, Q., Wang, L., Yang, L., 2022. Decision-making on the selection of clean energy technology for green ships based on the rough set and TOPSIS method. J. Mar. Sci. Eng. 10 (5), 579.
Zaman, K., Rangavajhala, S., McDonald, M.P., Mahadevan, S., 2011. A probabilistic approach for representation of interval uncertainty. Reliab. Eng. Syst. Saf. 96 (1), 117–130.